Title

Fructose-1,6-bisphosphatase is a nonenzymatic safety valve that curtails AKT activation to prevent insulin hyperresponsiveness

Journal

Cell Metabolism, 35(6)

ISSN

1550-4131

Authors

Gu, Li

Zhu, Yahui

Watari, Kosuke

et al.

Publication Date

2023-06-01

DOI

10.1016/j.cmet.2023.03.021

Article

Cell Metabolism

Fructose-1,6-bisphosphatase is a nonenzymatic safety valve that curtails AKT activation to prevent insulin hyperresponsiveness

Graphical abstract

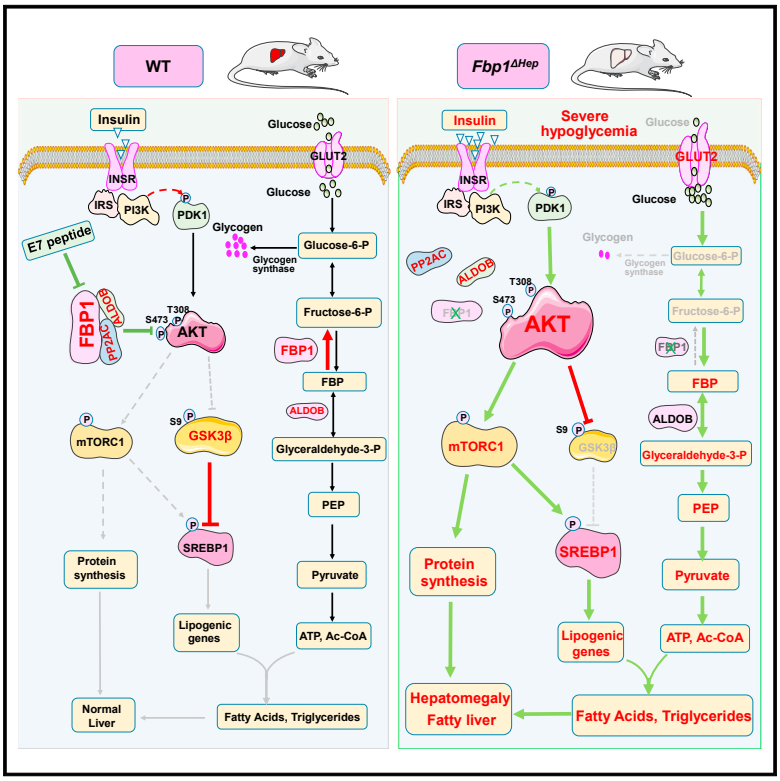

Highlights

- FBP1 deficiency causes hypoglycemia, hepatomegaly, hepatosteatosis, and hyperlipidemia
- FBP1 prevents insulin hyperresponsiveness independently of its catalytic activity
- FBP1 associates with PP2A-C and ALDOB and AKT to accelerate AKT dephosphorylation
- A complex disrupting FBP1-derived E7 peptide ameliorates diet-induced insulin resistance

Authors

Li Gu, Yahui Zhu, Kosuke Watari, ..., Alan R. Saltiel, M. Celeste Simon, Michael Karin

Correspondence

karinoffice@ucsd.edu

In brief

Gu et al. report that mice lacking hepatocyte fructose 1,6 bisphosphatase (FBP1, FBP'ase) exhibit low glycogen stores and fasting-induced hypoglycemia, hepatomegaly, hepatosteatosis, and hyperlipidemia, which is also displayed by FBP1-deficient humans. Apart from its FBP'ase activity required for gluconeogenesis, FBP1 non-enzymatically blunts insulin-induced AKT activation by forming a complex with AKT, PP2A-C, and aldolase B, which accelerates AKT dephosphorylation. Accordingly, inhibition of AKT hyperactivation reversed hepatomegaly, hepatosteatosis, and hyperlipidemia. A C-terminal FBP1 peptide that disrupts its binding to AKT and PP2A-C reverses diet-induced insulin resistance by restoring insulin sensitivity.

Gu et al., 2023, Cell Metabolism *35*, 1–13
June 6, 2023
https://doi.org/10.1016/j.cmet.2023.03.021

CellPress

Please cite this article in press as: Gu et al., Fructose-1,6-bisphosphatase is a nonenzymatic safety valve that curtails AKT activation to prevent insulin hyperresponsiveness, Cell Metabolism (2023), https://doi.org/10.1016/j.cmet.2023.03.021

Cell Metabolism

CellPress

Article

Fructose-1,6-bisphosphatase is a nonenzymatic safety valve that curtails AKT activation to prevent insulin hyperresponsiveness

Li Gu,[1,11] Yahui Zhu,[2,11] Kosuke Watari,[1] Maiya Lee,[1] Junlai Liu,[1] Sofia Perez,[1] Melinda Thai,[1] Joshua E. Mayfield,[3] Bichen Zhang,[4] Karina Cunha e Rocha,[4] Fuming Li,[5,6,7] Laura C. Kim,[5,6] Alexander C. Jones,[3] Igor H. Wierzbicki,[3] Xiao Liu,[4,8] Alexandra C. Newton,[3] Tatiana Kisseleva,[8] Jun Hee Lee,[9] Wei Ying,[4] David J. Gonzalez,[3,10] Alan R. Saltiel,[4] M. Celeste Simon,[5,6] and Michael Karin[1,12,*]

[1]Laboratory of Gene Regulation and Signal Transduction, Departments of Pharmacology and Pathology, School of Medicine, University of California, San Diego, La Jolla, CA 92093, USA
[2]School of Medicine, Chongqing University, Chongqing 400030, China
[3]Department of Pharmacology, University of California, San Diego, La Jolla, CA 92093, USA
[4]Division of Endocrinology & Metabolism, Department of Medicine, University of California, San Diego, La Jolla, CA 92093, USA
[5]Abramson Family Cancer Research Institute, Perelman School of Medicine, University of Pennsylvania, Philadelphia, PA 19104, USA
[6]Department of Cell and Developmental Biology, University of Pennsylvania, Philadelphia, PA 19104, USA
[7]Shanghai Key Laboratory of Metabolic Remodeling and Health, Institute of Metabolism and Integrative Biology, Fudan University, Shanghai 200438, China
[8]Department of Surgery, University of California, San Diego, La Jolla, CA 92093, USA
[9]Department of Molecular and Integrative Physiology, University of Michigan Medical School, Ann Arbor, MI 48109, USA
[10]Skaggs School of Pharmacy and Pharmaceutical Sciences, University of California, San Diego, La Jolla, CA, USA
[11]These authors contributed equally
[12]Lead contact
*Correspondence: karinoffice@ucsd.edu
https://doi.org/10.1016/j.cmet.2023.03.021

SUMMARY

Insulin inhibits gluconeogenesis and stimulates glucose conversion to glycogen and lipids. How these activities are coordinated to prevent hypoglycemia and hepatosteatosis is unclear. Fructose-1,6-bisphosphatase (FBP1) is rate controlling for gluconeogenesis. However, inborn human FBP1 deficiency does not cause hypoglycemia unless accompanied by fasting or starvation, which also trigger paradoxical hepatomegaly, hepatosteatosis, and hyperlipidemia. Hepatocyte FBP1-ablated mice exhibit identical fasting-conditional pathologies along with AKT hyperactivation, whose inhibition reversed hepatomegaly, hepatosteatosis, and hyperlipidemia but not hypoglycemia. Surprisingly, fasting-mediated AKT hyperactivation is insulin dependent. Independently of its catalytic activity, FBP1 prevents insulin hyperresponsiveness by forming a stable complex with AKT, PP2A-C, and aldolase B (ALDOB), which specifically accelerates AKT dephosphorylation. Enhanced by fasting and weakened by elevated insulin, FBP1:PP2A-C:ALDOB:AKT complex formation, which is disrupted by human FBP1 deficiency mutations or a C-terminal FBP1 truncation, prevents insulin-triggered liver pathologies and maintains lipid and glucose homeostasis. Conversely, an FBP1-derived complex disrupting peptide reverses diet-induced insulin resistance.

INTRODUCTION

Insulin is the master regulator of glucose homeostasis, keeping its blood concentration within a narrow range during fasting and feeding.[1] A major site of insulin action is the liver, where it stimulates glucose uptake, glycolysis, and glucose conversion to fatty acids (FAs) and glycogen while inhibiting glucose output by blocking glycogenolysis (GL) and gluconeogenesis (GNG).[2,3] How these activities are integrated and regulated to prevent fatal hypoglycemia and avoid hepatosteatosis and hyperlipidemia, metabolic disorders that affect 30% of American adults, is not entirely clear. The key insulin effector that controls glucose and lipid metabolism during the fed state is the AKT (AKT serine/threonine kinase)-phosphoinositide-3-kinase (PI3K) pathway,[4,5] but whether and how AKT is specifically deactivated during fasting is unknown.

Although not a direct target for insulin signaling, fructose (F) 1,6 bisphosphatase 1 (FBP1) is rate controlling for GNG, converting F1,6-P_2 to F6-P, which is then converted to glucose (G) 6-P by phosphoglucoseisomerase (PGI).[6,7] FBP1 deficiency is a rare inborn metabolic error (OMIM:229700), which causes severe hypoglycemia, lactic acidosis, seizures, hepatomegaly,

Please cite this article in press as: Gu et al., Fructose-1,6-bisphosphatase is a nonenzymatic safety valve that curtails AKT activation to prevent insulin hyperresponsiveness, Cell Metabolism (2023), https://doi.org/10.1016/j.cmet.2023.03.021

hyperlipidemia, hepatosteatosis, and liver damage in carbohydrate starved, but not fed, infants.[8–10] Although hypoglycemia and lactic acidosis are probably caused by low glycogen stores and abrogated GNG, there is no simple biochemical explanation for the hepatomegaly and elevated hepatic lipogenesis, which also affect non-starved older FBP1-deficient individuals.[8] We investigated hepatocyte-specific *Fbp1* knockout mice (*Fbp1*$^{\Delta Hep}$), initially generated for understanding FBP1's tumor suppressive function in hepatocellular carcinoma (HCC),[11] and found fasted *Fbp1*$^{\Delta Hep}$ mice to be phenotypically and metabolically identical to starved FBP1-deficient infants. In addition to low glycogen stores and severe hypoglycemia, these mice manifest fasting-induced liver pathologies, including hepatomegaly, hepatosteatosis, and hyperlipidemia. Unexpectedly and independently of its catalytic activity, we discovered that FBP1 is a critical regulator of insulin signaling, serving as an endogenous "safety valve" that prevents insulin hyperresponsiveness and balances glucose and lipid metabolism. FBP1 negatively controls insulin signaling by nucleating a stable multiprotein complex, which also contains aldolase B (ALDOB), an enzyme that acts upstream to FBP1 in the GNG pathway (Figure S1A), the catalytic subunit of protein phosphatase 2A (PP2A-C), which dephosphorylates AKT,[12] and AKT, the key effector of insulin signaling.[5] Complex formation, which keeps AKT activation in check, is enhanced by fasting and weakened during the fed state by insulin. Defective complex assembly causes hyperresponsiveness to the small amounts of insulin that are released in response to lipolysis-generated free FAs (FFAs), thereby triggering hepatosteatosis and hyperlipidemia.[13] Conversely, pharmacological complex disruption with an FBP1-derived peptide reversed diet-induced insulin resistance.

RESULTS

Hypoglycemia, hepatomegaly, fatty liver, and hyperlipidemia in fasted *Fbp1*$^{\Delta Hep}$ mice

To understand the metabolic impact of FBP1 deficiency and its biochemical sequalae, we crossed *Fbp1*$^{F/F}$ and *Alb-Cre* mice to generate *Fbp1*$^{\Delta Hep}$ mice. At 8 weeks of age and after a 16 h overnight fast, *Fbp1*$^{\Delta Hep}$, but not *Fbp1*$^{F/F}$, mice exhibited hepatomegaly, hepatosteatosis, severe hypoglycemia, hyperlipidemia, and signs of liver damage (elevated AST:ALT ratio) (Figures 1A–1I). Weights of other tissues were not altered (Figure S1B). Hepatomegaly was due to hypertrophy rather than hyperplasia (Figures S1C and S1D). Elevated lipolysis was unlikely to be the cause of hepatosteatosis because adipose tissue mRNAs encoding hormone-sensitive lipase (HSL) and adipose triglyceride lipase (ATGL) were insignificantly affected by *Fbp1* ablation (Figure S1E). Despite hypoglycemia, the *Fbp1*$^{\Delta Hep}$ livers contained more NADPH (nicotinamide adenine dinucleotide phosphate reduced), ATP, and acetyl-CoA, which support lipid synthesis, than *Fbp1*$^{F/F}$ livers contained (Figures 1J and S1F–S1H). No genotype-related differences in serum insulin or glucagon were observed in the fast state, although serum lactate was elevated in fasted *Fbp1*$^{\Delta Hep}$ mice (Figures S1I–S1K). Consistent with periodic acid Schiff (PAS) staining, hepatic glycogen and G6-P were reduced (Figures 1B, S1L, and S1M). Interestingly, even a mere 4-h fast caused mild hepatomegaly, hepatosteatosis, hypoglycemia, hyperlipidemia, signs of liver injury, and elevated hepatic NADPH:NADP (nicotinamide adenine dinucleotide phosphate) ratio and ATP in *Fbp1*$^{\Delta Hep}$ mice (Figures 1K–1T, S1N, and S1O). No significant differences in the weights of other tissues or lipolytic enzyme mRNAs were observed (Figures S1P and S1Q). Immunoblot (IB) analysis showed insignificant differences in HSL and ATGL phosphorylation in epididymal white adipose tissue (eWAT) after the 4-h fast (Figure S1R), further ruling out enhanced lipolysis as the basis for the observed metabolic abnormalities. The short 4 h fast still led to elevated serum lactate in *Fbp1*$^{\Delta Hep}$ mice but little genotype-related differences in serum insulin and glucagon (Figures S1S–S1U). Lastly, hepatic glycogen and G6-P were significantly lower in *Fbp1*$^{\Delta Hep}$ mice than in *Fbp1*$^{F/F}$ mice (Figures 1L, S1V, and S1W). In short, the metabolic phenotypes of hepatic steatosis, hypoglycemia, hepatomegaly, and hyperlipidemia associated with FBP1 deficiency appeared quickly within 4 h of fasting.

Fasted *Fbp1*$^{\Delta Hep}$ mice exhibit enhanced AKT-mTOR signaling and *de novo* lipogenesis

Fasted (16 h) *Fbp1*$^{\Delta Hep}$ livers and primary mouse hepatocytes showed enhanced AKT S473 and T308 and GSK3β S9 phosphorylations, loss of AMPK (Adenosine 5′-monophosphate [AMP]-activated protein kinase) T172 phosphorylation, and elevated S6 and p70 S6 kinase (p70S6K) phosphorylations, suggesting mTORC1 (mechanistic target of rapamycin kinase complex 1) activation (Figures 2A and S2A). Consistent with hepatosteatosis, previous findings,[11] and mTORC1 and p70S6K activation,[14] nuclear/mature (m) SREBP1c was strongly elevated in fasted *Fbp1*$^{\Delta Hep}$ livers, along with its targets, ATP citrate lyase (ACLY), acetyl CoA carboxylase 1 (ACC1) and FA synthase (FASN), and the SREBP2 targets, HMG CoA synthase 1 (HMGCS1) and reductase (HMGCR) (Figures 2B–2D). The lipid transporter CD36, Glut2, pyruvate kinase M2 (PKM2), phosphogluconate dehydrogenase (PGD), transketolase (TKT), malic enzyme 1 (ME1), methylenetetrahydrofolate dehydrogenase 2 (MTHFD2), phosphoribosyl pyrophosphate amidotransferase (PPAT), and 1,4-α-glucan branching enzyme 1 (GBE1) mRNAs were elevated, whereas carnitine palmitoyl transferases 1a and 2 (CPT1a, CPT2) mRNAs, involved in β-oxidation, were reduced (Figures 2E–2G). Carbohydrate-response-element-binding protein (ChREBP), whose overexpression promotes hepatic steatosis while improving insulin sensitivity,[15] was also elevated in the cytoplasm and nucleus of *Fbp1*$^{\Delta Hep}$ livers and so was glucocorticoid receptor (GR) (Figure S2B).

GC-MS-based metabolomic analysis of ^{13}C-glucose-loaded livers revealed elevated glycolytic flux and decreased TCA (tricarboxylic acid)-cycle activity in fasted *Fbp1*$^{\Delta Hep}$ livers (Figures S2C–S2E), explaining the increase in serum lactate. ^{13}C-lactate tracing showed reduced lactate flux to F6-P and G6-P but enhanced lactate flux into TCA-cycle intermediates and amino acids (Figures 2H–2J, S2C, and S2F), correlating with reduced liver glycogen. D_2O tracing confirmed elevated *de novo* lipogenesis (DNL) in fasted *Fbp1*$^{\Delta Hep}$ mice (Figures 2K and 2L). Curiously, glycogen synthase 2 (GYS2) and its phosphorylated form (P-GS) were elevated in fasted *Fbp1*$^{\Delta Hep}$ livers (Figure S2G) despite their low glycogen content and the increase in inhibitory GSK3 phosphorylation, which should have increased GYS2 activity.[16] This suggested that diminished *Fbp1*$^{\Delta Hep}$ liver glycogen stores could

Please cite this article in press as: Gu et al., Fructose-1,6-bisphosphatase is a nonenzymatic safety valve that curtails AKT activation to prevent insulin hyperresponsiveness, Cell Metabolism (2023), https://doi.org/10.1016/j.cmet.2023.03.021

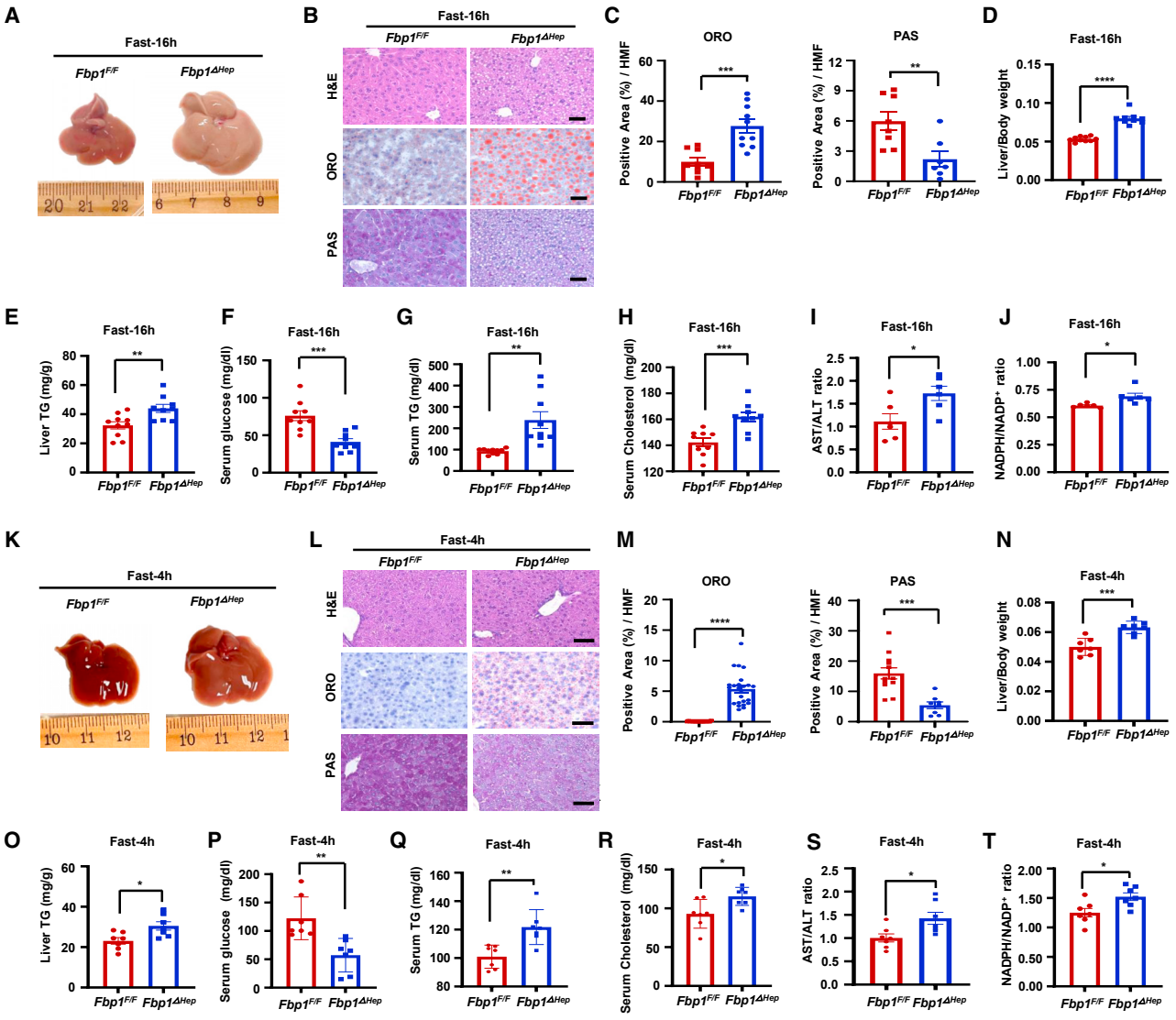

Figure 1. Hepatomegaly, hepatosteatosis, hypoglycemia in fasted *Fbp1*$^{\Delta Hep}$ mice

(A) Gross morphology of livers from 8-week-old *Fbp1*$^{F/F}$ and *Fbp1*$^{\Delta hep}$ mice fasted for 16 h.

(B) Hematoxylin and eosin (H&E), oil red O (ORO), and periodic acid Schiff (PAS) staining of liver sections from 1A (n = 8). Scale bars, 20 μm.

(C) ORO and PAS staining intensity per high-magnification-field (HMF) was determined by Image J from the slides shown in (B).

(D–H) Liver/body weight (D), liver triglycerides (TG) (E), and serum glucose (F), TG (G), and cholesterol (H) in the indicated mice (n = 9–10).

(I and J) Serum aspartate aminotransferase (AST) / alanine aminotransferase (ALT) ratio (I) and liver NADPH/NADP$^+$ ratio (J) in the indicated mice (n = 6).

(K) Gross morphology of livers from 8-week-old *Fbp1*$^{F/F}$ and *Fbp1*$^{\Delta hep}$ mice fasted for 4 h.

(L) H&E, ORO, and PAS staining of liver sections from (K) (n = 7). Scale bars, 20 μm.

(M) ORO and PAS staining intensity per HMF was determined by Image J analysis of the data in (L).

(N–R) Liver/body weight (N), liver TG (O), and serum glucose (P), TG (Q), and cholesterol (R) in the indicated mice (n = 7).

(S and T) Serum AST/ALT ratio (S) and liver NADPH/NADP$^+$ ratio (T) in the indicated mice (n = 7).

Data are presented as mean ± SEM. *p < 0.05, **p < 0.01, ***p < 0.001, ****p < 0.0001 (unpaired two-tailed t test).

be due to low G6-P, the key allosteric activator of GYS2,[17] which is generated by PGI from F6-P, whose production from lactate via GNG was reduced. Indeed, GYS activity was significantly lower in *Fbp1*$^{\Delta Hep}$ liver lysates relative to *Fbp1*$^{F/F}$ liver lysates (Figure S2H). This difference was indeed due to lower G6-P in the *Fbp1*$^{\Delta Hep}$ liver because when exogenous G6-P was added to the reaction mix GYS activity was higher in *Fbp1*$^{\Delta Hep}$ liver lysates, consistent with higher GYS2 abundance.

After a 4-h fast, *Fbp1*$^{\Delta Hep}$ livers also showed elevated AKT activation, GSK3β S9 phosphorylation, S6 and p70S6K phosphorylation, and reduced AMPK activation (Figure 2M). SREBP1 target mRNAs encoding ACLY, ACC1, and FASN were moderately elevated, along with the SREBP2 target HMGCR, the lipid transporter CD36, and the metabolic enzymes PKM2, PGD, TKT, ME1, and PPAT, whereas CPT2 mRNA was decreased (Figures 2N and S2I–S2L).

Please cite this article in press as: Gu et al., Fructose-1,6-bisphosphatase is a nonenzymatic safety valve that curtails AKT activation to prevent insulin hyperresponsiveness, Cell Metabolism (2023), https://doi.org/10.1016/j.cmet.2023.03.021

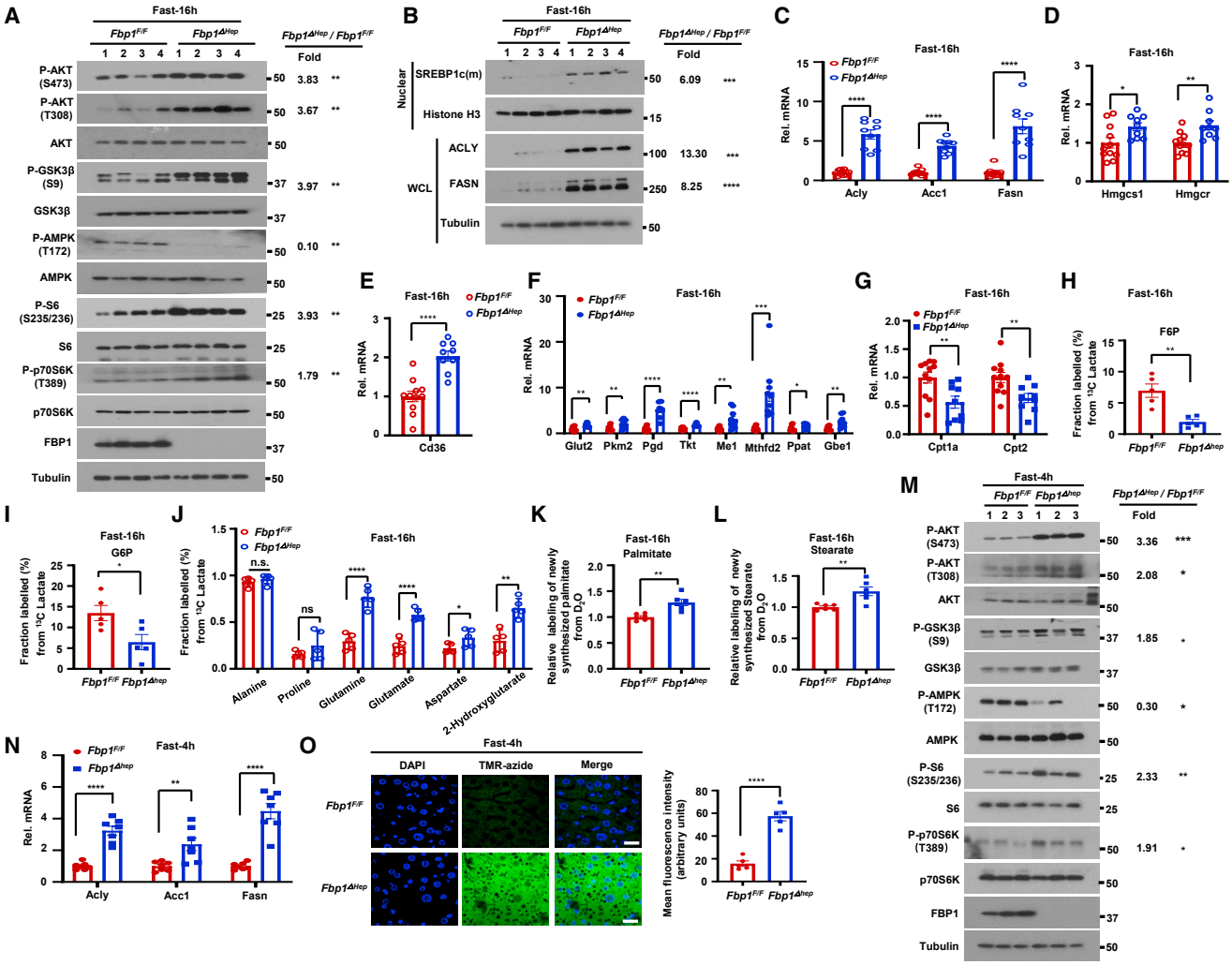

Figure 2. Fasted *Fbp1*$^{\Delta Hep}$ mice exhibit enhanced AKT-mTOR signaling and elevated *de novo* lipogenesis

(A) Immunoblot (IB) analysis of the indicated proteins in livers of 16-h-fasted 8-week-old *Fbp1*$^{F/F}$ and *Fbp1*$^{\Delta Hep}$ mice. Densitometric quantification of relative normalized protein ratios (*Fbp1*$^{\Delta Hep}$/*Fbp1*$^{F/F}$), and p values are shown on the right.

(B) IB analysis of indicated proteins in 16-h-fasted 8-week-old *Fbp1*$^{F/F}$ and *Fbp1*$^{\Delta Hep}$ mice (n = 4). Relative normalized protein ratios (*Fbp1*$^{\Delta Hep}$/*Fbp1*$^{F/F}$), and p values are shown on the right.

(C–G) Quantitative real-time PCR analysis of lipogenesis (C), cholesterol synthesis (D), lipid uptake (E), glycolysis, pentose phosphate pathway, glycogen synthesis (F), and β-oxidation (G) -related liver mRNAs from fasted 8-week-old *Fbp1*$^{F/F}$ and *Fbp1*$^{\Delta Hep}$ mice (n = 9–10).

(H–J) Fractional labeling of liver F6-P (H), G6-P (I), and amino acids (J) from ^{13}C-lactate tracing of 16-h-fasted 8-week-old *Fbp1*$^{F/F}$ and *Fbp1*$^{\Delta Hep}$ mice (n = 5).

(K and L) Relative deuterium incorporation into newly synthesized liver palmitate (C16:0) (K) and stearate (C18:0) (L) after 24 h of D_2O labeling (n = 4–6).

(M) IB analysis of indicated liver proteins from 4-h-fasted 8-week-old *Fbp1*$^{F/F}$ and *Fbp1*$^{\Delta Hep}$ mice. Relative normalized protein ratios (*Fbp1*$^{\Delta Hep}$/*Fbp1*$^{F/F}$), and p values are shown on the right.

(N) Quantitative real-time PCR analysis of lipogenesis related liver mRNAs from 4-h-fasted 8-week-old *Fbp1*$^{F/F}$ and *Fbp1*$^{\Delta Hep}$ mice (n = 7).

(O) Liver protein synthesis in 4-h-fasted 8-week-old *Fbp1*$^{F/F}$ and *Fbp1*$^{\Delta Hep}$ mice was imaged (left) by O-propargyl-puromycin (OPP, TMR-azide) incorporation (n = 5), and mean fluorescence intensity was quantified (right). Scale bars, 20 μm.

Data are presented as mean ± SEM. n.s., not significant, P ≥ 0.05,*p < 0.05, **p < 0.01, ***p < 0.001, ****p < 0.0001 (unpaired two-tailed t test). All blots are representative of at least 3 biological replicates.

Consistent with mTORC1 activation and hepatomegaly, protein synthesis measured with O-propargyl-puromycin (OP-puro) was strongly elevated in 4-h-fasted *Fbp1*$^{\Delta Hep}$ hepatocytes (Figure 2O) and so were nuclear ChREBP and GR (Figure S2M). Thus, the FBP1 deficiency results in rapid, fasting-induced upregulation of AKT-mTOR signaling, lipogenesis, and protein synthesis.

Of note, in the fed state, *Fbp1*$^{\Delta Hep}$ livers were barely different from *Fbp1*$^{F/F}$ livers, although the *Fbp1*$^{\Delta Hep}$ liver exhibited slight hepatomegaly, somewhat lower glycogen, and marginally elevated liver damage (Figures S3A–S3J). Serum parameters also did not differ between the two genotypes (Figures S3K–S3O). *Fbp1*$^{\Delta Hep}$ livers also showed increased ACLY and ME1 mRNAs, but mRNAs encoding other metabolic genes did not

Please cite this article in press as: Gu et al., Fructose-1,6-bisphosphatase is a nonenzymatic safety valve that curtails AKT activation to prevent insulin hyperresponsiveness, Cell Metabolism (2023), https://doi.org/10.1016/j.cmet.2023.03.021

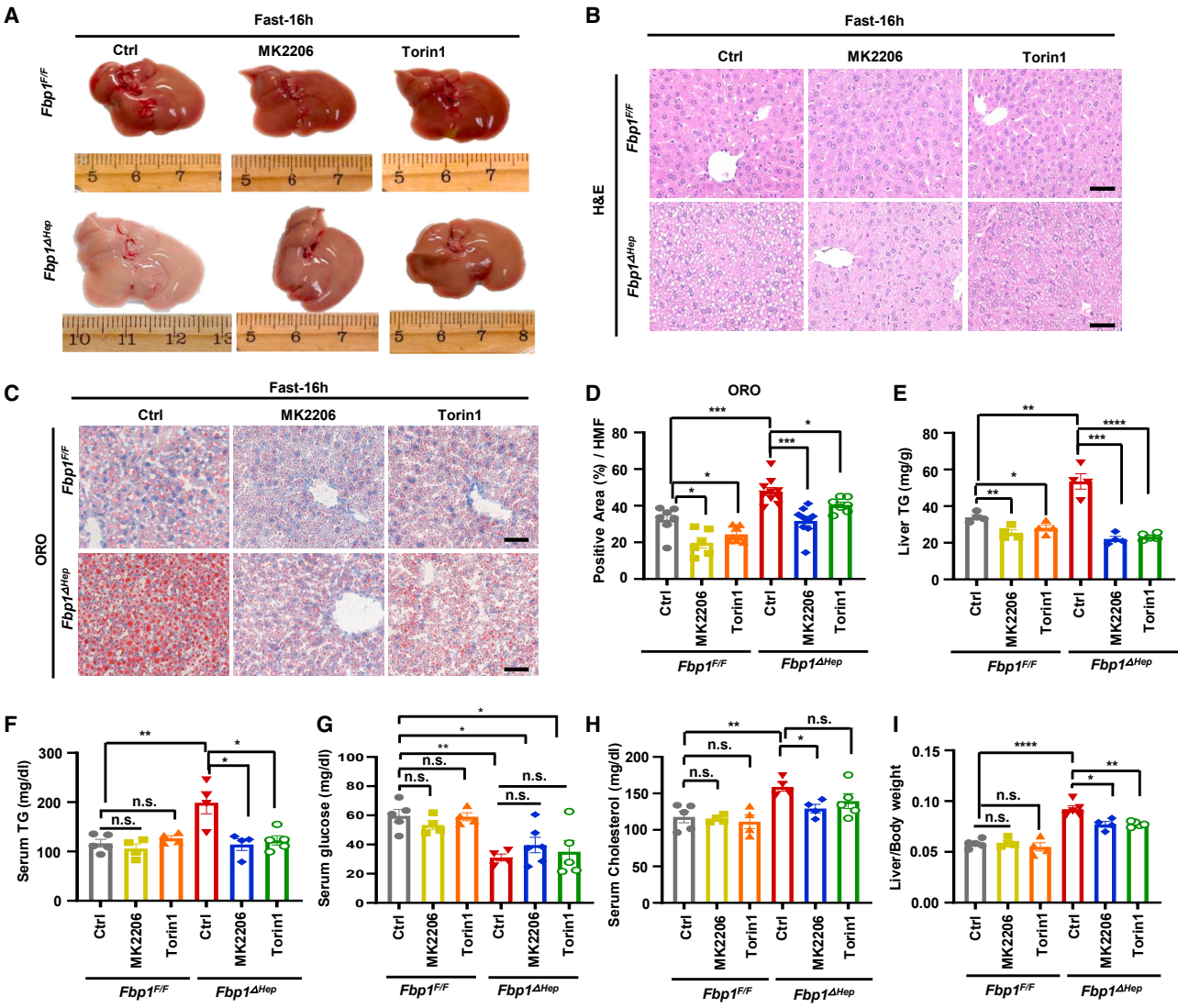

Figure 3. AKT inhibition attenuate hepatomegaly, hepatosteatosis, and hyperlipidemia but not hypoglycemia

(A) Gross liver morphology of 8-week-old *Fbp1*$^{F/F}$ and *Fbp1*$^{\Delta Hep}$ mice treated ± MK2206 (100 mg/kg) or Torin1 (10 mg/kg), followed by 16 h fast before sacrifice. (B–D) H&E (B) and ORO staining (C) of liver sections from (A) (n = 4–5). Scale bars, 20 μm. ORO staining intensity per HMF was determined by Image J (D). (E–I) Liver TG (E), serum TG (F), serum glucose (G), serum cholesterol (H), and liver/body weight ratio (I) in indicated mice (n = 4–5).

Data are presented as mean ± SEM. n.s., not significant, $p \geq 0.05$. *$p < 0.05$, **$p < 0.01$, ***$p < 0.001$, ****$p < 0.0001$ (unpaired two-tailed t test).

differ from those in *Fbp1*$^{F/F}$ livers (Figures S3P–S3T). No changes in GYS2 and P-GS amounts were observed (Figure S3U).

AKTi and mTORCi attenuate lipogenesis and protein synthesis but not hypoglycemia

To determine whether elevated AKT or mTORC1 activities contribute to the metabolic abnormalities in fasted *Fbp1*$^{\Delta Hep}$ mice, we treated the mice with AKT (MK2206) or mTORC1/2 (Torin1) inhibitors 28 and 4 h before fasting. Both inhibitors prevented hepatosteatosis and hypertriglyceridemia, reducing them to levels seen in drug-treated, fasted *Fbp1*$^{F/F}$ mice, but had no effect on hypoglycemia (Figures 3A–3G). Serum cholesterol was reduced by MK2206 but not by Torin1 (Figure 3H). The two inhibitors partially abrogated hepatomegaly (Figures 3A and 3I) and blunted the fasting-induced increase in protein synthesis but did not alter serum insulin (Figures S4A–S4C). As expected, MK2206 and Torin1 (which also inhibits mTORC2 that acts upstream to AKT) blocked fasting-induced AKT, ribosomal protein S6 and GSK3β phosphorylation, and blunted SREBP1c, ACLY, FASN, HMGCR, and CD36 mRNA expression (Figures S4D and S4E).

Catalytically inactive FBP1 prevents hepatomegaly, steatosis, and hyperlipidemia

In addition to catalyzing GNG, FBP1 non-enzymatically inhibits HIF-1 activity.[6] AAV8 (adeno-associated virus 8)-mediated re-expression of WT FBP1 or catalytically inactive FBP1^{E98A} in *Fbp1*$^{\Delta Hep}$ hepatocytes had an effect akin to AKTi treatment,

Please cite this article in press as: Gu et al., Fructose-1,6-bisphosphatase is a nonenzymatic safety valve that curtails AKT activation to prevent insulin hyperresponsiveness, Cell Metabolism (2023), https://doi.org/10.1016/j.cmet.2023.03.021

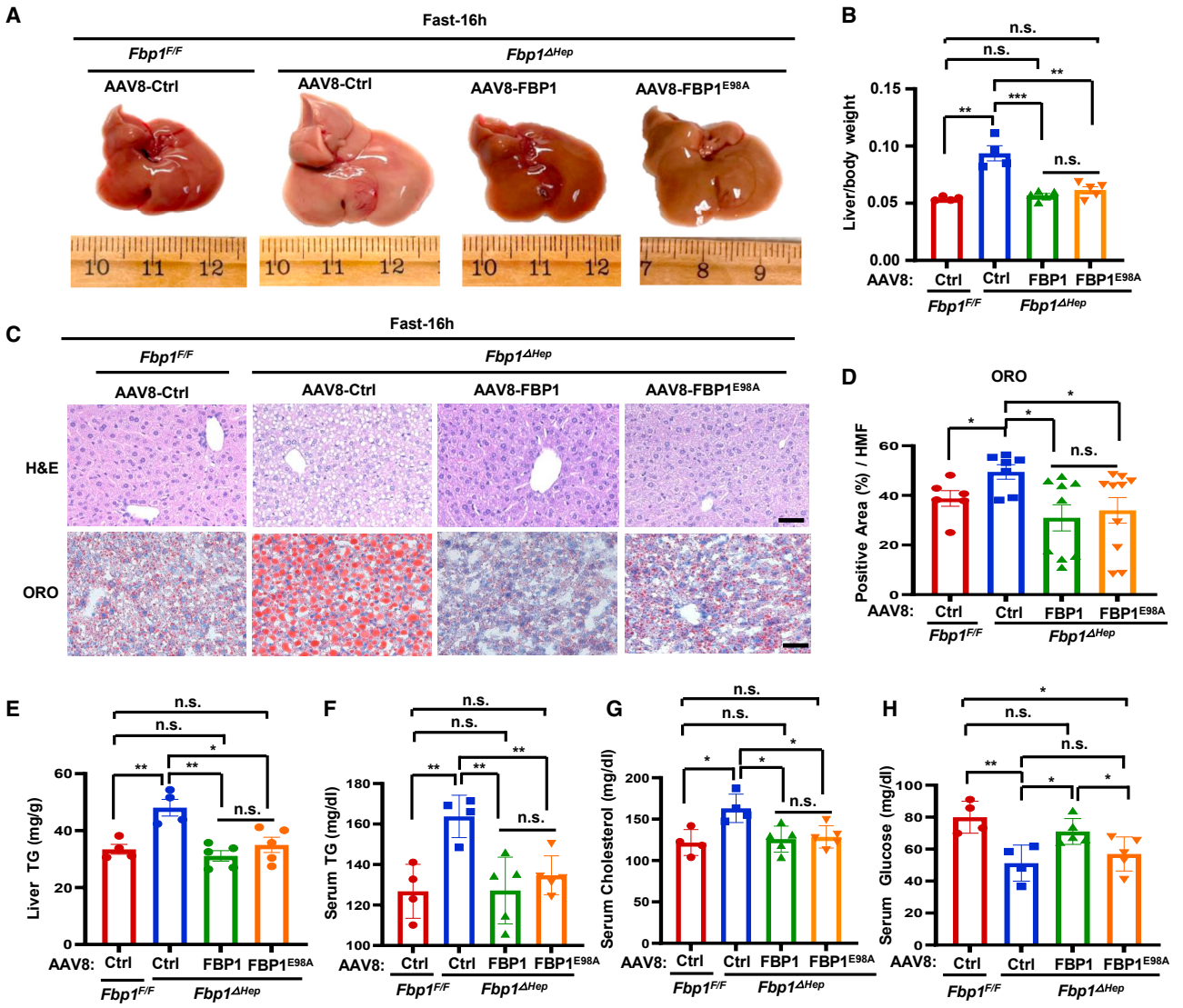

Figure 4. Inactive FBP1 prevents hepatomegaly, steatosis, and hyperlipidemia

(A) Gross liver morphology of 8-week-old *Fbp1*$^{F/F}$ and *Fbp1*$^{\Delta Hep}$ transduced with AAV8-Ctrl, AAV8-FBP1, and AAV8-FBP1^{E98A}, followed by 16 h fast before sacrifice at 3 week post-AAV8 infection (n = 4–5).

(B) Liver/body weight ratio in above mice (n = 4–5).

(C and D) H&E and ORO staining of liver sections from (A) (n = 4–5) (C). Scale bars, 20 μm. ORO staining intensity per HMF determined by Image J (D).

(E–H) Liver TG (E), serum TG (F), serum cholesterol (G), and serum glucose (H) in the indicated mice (n = 4–5).

Data are mean ± SEM. n.s., not significant, $p \geq 0.05$, *$p < 0.05$, **$p < 0.01$, ***$p < 0.001$ (unpaired two-tailed t test).

blunting fasting-induced hepatomegaly, hepatosteatosis, and hyperlipidemia and reducing lipogenic gene expression, although, as expected, FBP1^{E98A} did not obliterate hypoglycemia (Figures 4A–4H, S5A, and S5B). AAV8-mediated FBP1 or FBP1^{E98A} re-expression largely suppressed AKT activation and GSK3β S9 phosphorylation (Figures S5C and S5D).

To elucidate how FBP1 regulated AKT activation, we used mass spectrometry (MS) as an unbiased tool to identify FBP1 binding proteins. ALDOB, AKT1, and PP2A-C ranked as the top FBP1-interacting partners present in HA-FBP1 immunoprecipitates (IPs) isolated from AAV8-FBP1 transduced *Fbp1*$^{\Delta Hep}$ livers (Figure S5E). *Fbp1*$^{\Delta Hep}$ livers transduced with AAV8-Ctrl served as a negative control. Of note, no PP2A regulatory subunits coIP'ed with FBP1.

FBP1 associates with PP2A-C and ALDOB to bind AKT and inhibit its activation

Next, we examined whether PP2A-C and ALDOB were part of the AKT inhibitory mechanism triggered by FBP1. FBP1-deficient individuals exhibit mild hereditary fructose intolerance (HFI),[8,10] a metabolic disorder associated with ALDOB deficiency (OMIM;229600), which blocks F1,6-P_2 breakdown.[18,19] ALDOB deficiency also causes hepatomegaly, hepatosteatosis, and liver damage.[20,21] This phenotypic overlap suggested that

Please cite this article in press as: Gu et al., Fructose-1,6-bisphosphatase is a nonenzymatic safety valve that curtails AKT activation to prevent insulin hyperresponsiveness, Cell Metabolism (2023), https://doi.org/10.1016/j.cmet.2023.03.021

CellPress

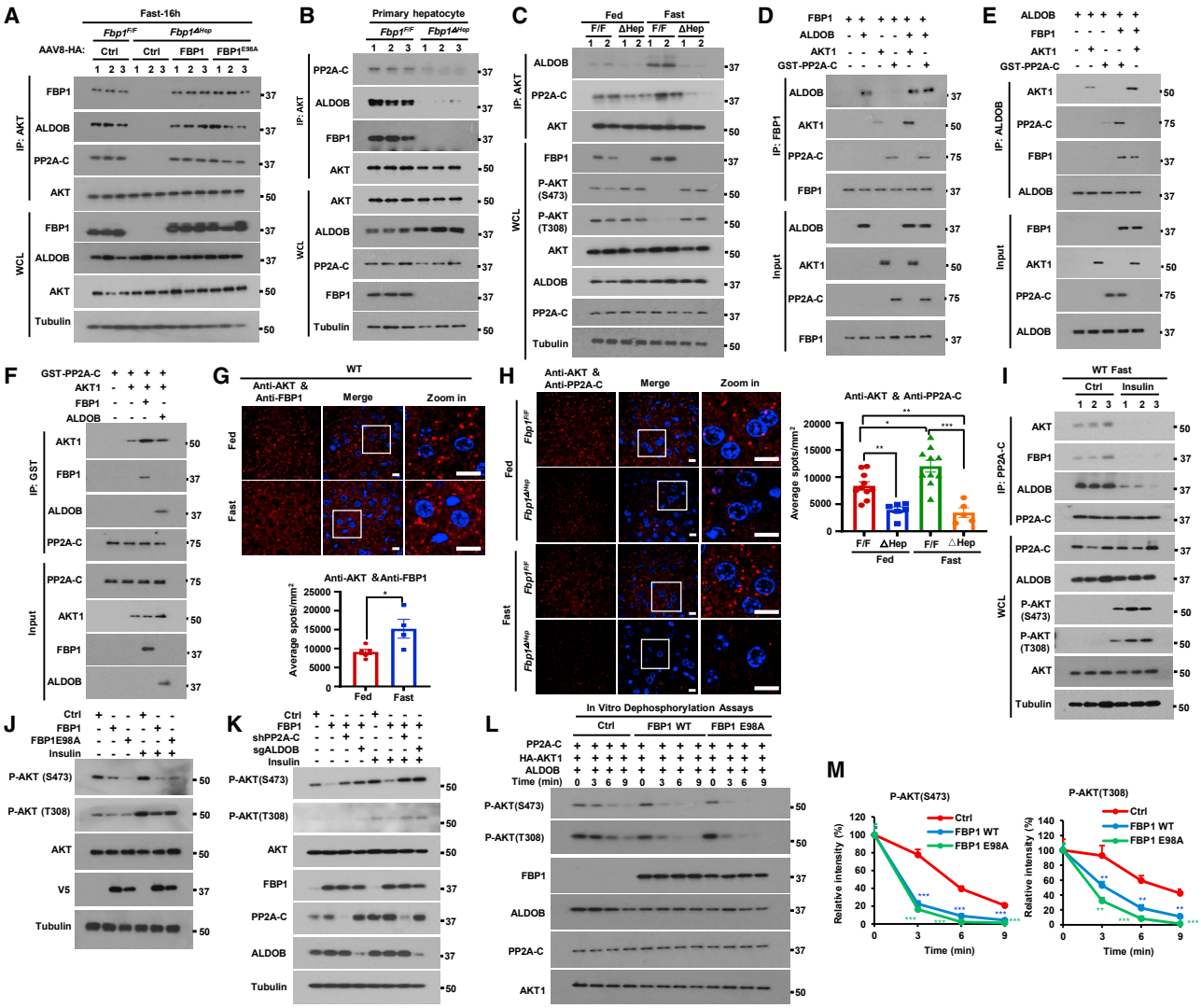

Figure 5. FBP1 associates with PP2A-C and ALDOB to inhibit AKT activation

(A) IP analysis of liver lysates from *Fbp1*$^{F/F}$ and *Fbp1*$^{\Delta Hep}$ mice transduced with AAV8-Ctrl, AAV8-FBP1, and AAV8-FBP1^{E98A} (n = 3). The gel separated IPs were IB'ed with the indicated antibodies.

(B) IP of primary mouse hepatocytes isolated from 16-h-fasted *Fbp1*$^{F/F}$ and *Fbp1*$^{\Delta Hep}$ mice (n = 3). The gel separated IPs were IB'ed with the indicated antibodies.

(C) IP analysis of liver lysates from fed or 16-h-fasted 8-week-old *Fbp1*$^{F/F}$ and *Fbp1*$^{\Delta Hep}$ mice. The gel separated IPs were IB'ed with the indicated antibodies.

(D–F) *In vitro* associations between FBP1 (D), ALDOB (E), and GST-PP2A-C (F) with the indicated recombinant proteins. The gel separated IPs were IB'ed with the indicated antibodies.

(G and H) PLA of AKT-FBP1 (G, top) and AKT-PP2A-C (H, left) interactions in liver sections of fed or 16-h-fasted 8-week-old *Fbp1*$^{F/F}$ and *Fbp1*$^{\Delta Hep}$ mice (n = 5–8). Scale bars, 10 μm. Quantification of representative stained tissues (G, bottom and H, right).

(I) IP of liver lysates of WT mice treated ± insulin (0.5 U/kg) after an overnight fast (n = 3). The gel separated IP's were IB'ed with indicated antibodies.

(J and K) IB analysis of Huh7 cells stably transfected with the indicated vectors and stimulated or not with insulin (100 nM) for 1 h after 6 h of serum starvation.

(L and M) *In vitro* dephosphorylation of phosphorylated HA-AKT1 isolated from insulin stimulated Huh7 cells and incubated with active-PP2A-C in the presence or absence of indicated recombinant proteins. The reactions were IB analyzed with the indicated antibodies (L). Relative intensity of P-AKT (S473) and P-AKT (T308) was determined by densitometry (M).

Data are presented as mean ± SEM. *p < 0.05, **p < 0.01, ***p < 0.001 (unpaired two-tailed t test).

FBP1 may regulate AKT activity through its interaction with ALDOB, which was also detected in previous studies.[22] Consistent with our MS analysis, ALDOB was reported to recruit PP2A-C to AKT in HCC cells and enhance AKT dephosphorylation.[23] Indeed, we confirmed that ectopically expressed WT and catalytically inactive FBP1^{E98A} interacted with AKT1, AKT2, ALDOB, and PP2A-C in 293T cells and that ectopic ALDOB IPs contained endogenous AKT1 and FBP1 (Figures S6A and S6B). Likewise, ectopic PP2A-C interacted with AKT1 and FBP1, which enhanced the AKT1-PP2A-C interaction (Figure S6C). Ectopic WT or FBP1^{E98A} expression in Huh7 cells potentiated the interaction between AKT, ALDOB, and PP2A-C, but FBP1 or ALDOB silencing disrupted the interactions between AKT, PP2A-C, ALDOB, and FBP1 (Figures S6D–

Please cite this article in press as: Gu et al., Fructose-1,6-bisphosphatase is a nonenzymatic safety valve that curtails AKT activation to prevent insulin hyperresponsiveness, Cell Metabolism (2023), https://doi.org/10.1016/j.cmet.2023.03.021

S6F). These interactions were also confirmed in mouse liver; AKT IPs from *Fbp1*$^{F/F}$ or *Fbp1*$^{\Delta Hep}$ livers reconstituted with FBP1 or FBP1^{E98A} contained FBP1, ALDOB, and PP2A-C (Figure 5A). Similar results were obtained when AKT was IP'ed from primary mouse hepatocytes, in which the absence of FBP1 diminished the association of AKT with ALDOB and PP2A-C (Figure 5B), indicating that FBP1 plays a pivotal role in complex formation. Formation of the FBP1-dependent FBP1:PP2A-C:ALDOB:AKT complex was enhanced by fasting (Figures 5C, S6G, and S6H). *In vitro* binding experiments confirmed assembly of the FBP1:PP2A-C:ALDOB:AKT complex using purified recombinant proteins, revealing that FBP1 first binds ALDOB and PP2A-C, and weakly to AKT1 (Figures 5D–5F). Addition of ALDOB and PP2A-C enhanced AKT1 binding and although ALDOB and PP2A-C interacted with AKT1, these interactions were enhanced by FBP1. Gel filtration chromatography of *Fbp1*$^{F/F}$ liver lysates revealed co-elution of FBP1, AKT, PP2A-C, and ALDOB in a high molecular weight fraction, averaging 750–800 kDa, which was not seen in *Fbp1*$^{\Delta Hep}$ lysates (Figures S6I and S6J).

Proximity ligation assays (PLAs) confirmed formation of the FBP1:PP2A-C:ALDOB:AKT complex in mouse liver and the pivotal role of FBP1 in coordinating ALDOB and PP2A-C recruitment to AKT (Figures 5G, 5H, and S6K–S6N). The interactions between FBP1, ALDOB, PP2A-C, and AKT were enhanced by fasting and weakened by feeding or insulin (Figures 5G–5I and S6K–S6T). FBP1 knockdown in the kidney epithelial cell line HK-2 or the colon carcinoma-derived CaCo-2 cell line also augmented AKT activation with and without insulin (Figure S6U). Ectopic expression of either WT FBP1 or FBP1^{E98A} in HCC cells inhibited basal and insulin-stimulated AKT S473 phosphorylation in a PP2A-C- and ALDOB-dependent manner (Figures 5J and 5K). *In vitro* dephosphorylation assay using active AKT1 as a substrate showed that either FBP1 variant stimulated time-dependent S473 and T308 dephosphorylation in an ALDOB-dependent manner (Figures 5L, 5M, and S6V). Dephosphorylation of another PP2A substrate was not affected by FBP1 (Figure S6W).

Fbp1$^{\Delta Hep}$ mice are hyperresponsive to insulin

As people and mice with obesity show insulin resistance, which interferes with AKT activation, we checked how HFD (high-fat diet) consumption affects the FBP1-PP2A-C-ALDOB-AKT complex. WB (western blot) and PLA showed that HFD enhanced FBP1 and ALDOB expression, as well as complex formation and inhibited AKT activation in WT mice (Figures S7A–S7D). We also fed *Fbp1*$^{F/F}$ and *Fbp1*$^{\Delta Hep}$ mice HFD for 12 weeks. Although weight gain was nearly identical between the two, *Fbp1*$^{\Delta Hep}$ mice exhibited higher liver to body weight ratio (Figures S7E and S7F), hepatomegaly, and enhanced hepatosteatosis, but less liver glycogen, than *Fbp1*$^{F/F}$ mice (Figures 6A–6C). Although HFD-fed *Fbp1*$^{\Delta Hep}$ mice were protected from obesity-related hyperglycemia, their liver and serum triglycerides (TGs) and cholesterol were elevated (Figures 6D–6G). Glucose tolerance test (GTT) showed that HFD-fed *Fbp1*$^{\Delta Hep}$ mice were more glucose tolerant than *Fbp1*$^{F/F}$ mice, although insulin levels did not differ between the two (Figures 6H and S7G). Insulin tolerance test (ITT) confirmed insulin hypersensitivity in HFD-fed *Fbp1*$^{\Delta Hep}$ mice (Figure 6I), whose liver contained more phosphorylated AKT and GSK3β than the *Fbp1*$^{F/F}$ liver (Figure 6J). Insulin administration to either HFD- or normal chow (NCD)-fed *Fbp1*$^{F/F}$ and *Fbp1*$^{\Delta Hep}$ mice resulted in higher AKT phosphorylation, under both HFD and NCD feeding and a considerable and sustained drop in blood glucose in NCD-fed *Fbp1*$^{\Delta Hep}$ mice (Figures 6K, 6L, and S7H). GTT and ITT indicated that both FBP1 and FBP1^{E98A} re-expression decreased glucose tolerance and insulin hypersensitivity (Figures S7I and S7J), even though insulin levels during GTT did not differ between the two (Figures S7K and S7L). *Fbp1*$^{\Delta Hep}$ mice were less pyruvate tolerant and this was reversed by AAV-FBP1, but not AAV-FBP1^{E98A}, re-expression (Figures S7M and S7N). Suppression of insulin-induced AKT activation was also seen in human hepatocytes, where FBP1 silencing enhanced insulin-induced AKT activation in a dose- and time-dependent manner (Figures 6M and S7O).

Insulin concentrations are higher in the fed state relative to the fasted state, making us wonder how fasting triggers AKT activation in *Fbp1*$^{\Delta Hep}$ mice. Postulating that the fasting-induced increase in AKT activation, steatosis, and hepatomegaly in *Fbp1*$^{\Delta Hep}$ mice could be due to FA-stimulated insulin secretion as a consequence of fasting-induced lipolysis,[24] we injected *Fbp1*$^{F/F}$ and *Fbp1*$^{\Delta Hep}$ mice with high-dose streptozotocin (STZ) to destroy insulin producing β cells.[25] As expected, STZ treatment reduced blood insulin and increased blood glucose, which was slightly lower in *Fbp1*$^{\Delta Hep}$ mice than in *Fbp1*$^{F/F}$ mice after a 4 h fast (Figures S7P and S7Q). Importantly, STZ treatment blocked fasting-induced hepatomegaly, hyperlipidemia, AKT and GSK3β phosphorylation, and the increase in ACLY, ACC1, FASN, HMGCS1, HMGCR, and CD36 mRNA expression (Figures S7R–S7Y), indicating that the liver phenotypes manifested by fasted *Fbp1*$^{\Delta Hep}$ mice depend on insulin secretion from β cells.

A complex disrupting FBP1-derived peptide ameliorates insulin resistance

In addition to deletion and nonsense mutations that block FBP1 expression, human FBP1 deficiency can be caused by missense mutations.[9,26] We stably expressed FBP1 missense mutants in Huh7 cells and found most of them to be poorly expressed and devoid of catalytic activity (Figures 7A and S8A). Those variants that were expressed, R158W, G164S, N213K, and L329P, no longer inhibited insulin stimulated AKT phosphorylation (Figure 7A). Particularly interesting was FBP1^{L329P} in exon 7, which was relatively well expressed with only a partial loss of FBP1 catalytic activity but completely devoid of AKT inhibitory activity (Figures 7A, S8A, and S8B). Unlike WT FBP1 and FBP1^{E98A}, FBP1^{L329P} did not associate with AKT, ALDOB, and PP2A-C (Figure 7B). To further delineate FBP1 sequences mediating these interactions, we used FBP1 deletion mutants, ΔE1-ΔE7,[6] each lacking one *FBP1* exon (E) (Figure S8B). ΔE6 and ΔE7 did not bind AKT nor inhibited its activity and ΔE7 did not interact with PP2A-C, but ΔE1 was only defective in ALDOB binding (Figures 7C and S8C). These results suggest that FBP1 assembles the AKT inhibitory complex through separate and distinct contacts with AKT, PP2A-C, and ALDOB. To test whether a synthetic E7 peptide that binds AKT, or PP2A-C can disrupt the FBP1:PP2A-C:ALDOB:AKT complex and lead to AKT activation, we synthesized a peptide encompassing FBP1 AA (amino acid) 275–300 preceded by a TAT-derived cell-penetrating peptide (Figure S8D). According to AlphaFold structural prediction and docking analysis, the E7 peptide is alpha helical, assuming the

Please cite this article in press as: Gu et al., Fructose-1,6-bisphosphatase is a nonenzymatic safety valve that curtails AKT activation to prevent insulin hyperresponsiveness, Cell Metabolism (2023), https://doi.org/10.1016/j.cmet.2023.03.021

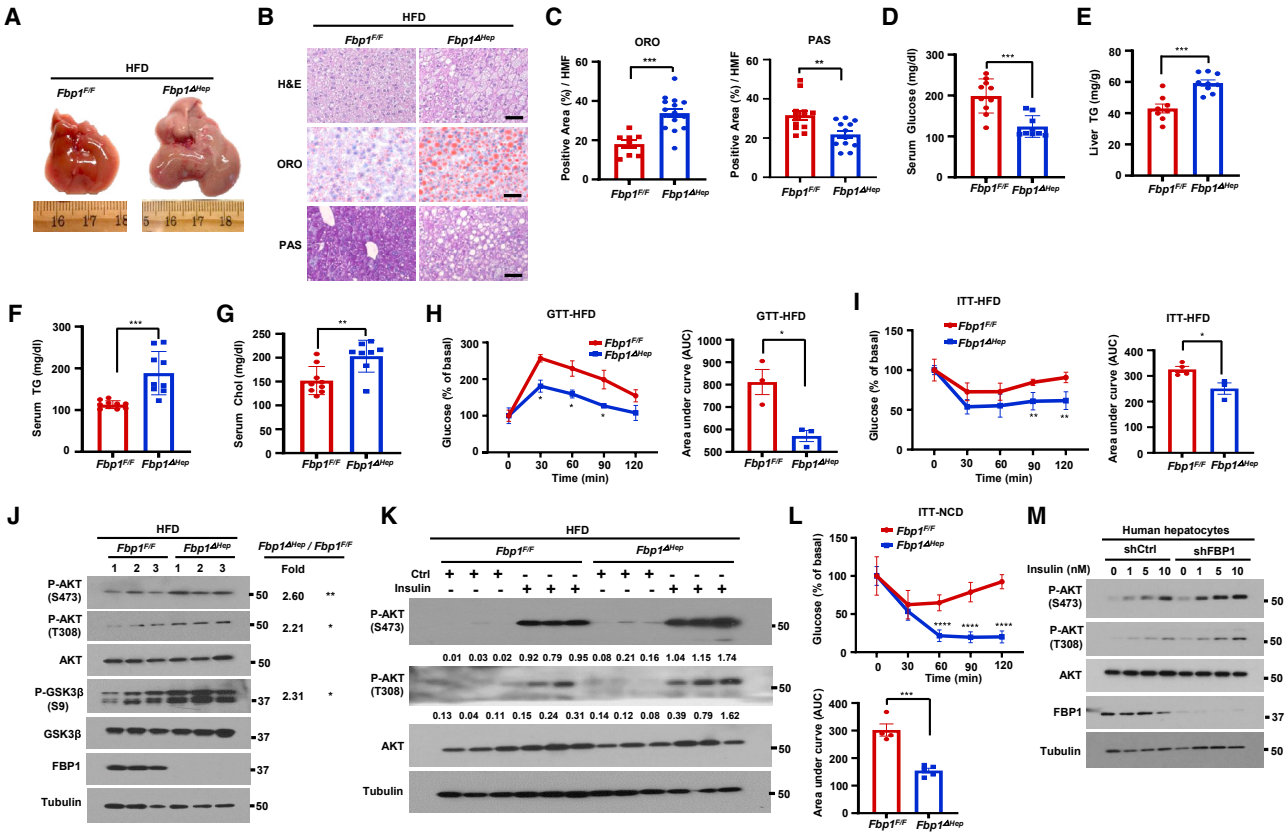

Figure 6. *Fbp1*$^{\Delta Hep}$ mice and FBP1-deficient human hepatocytes are insulin hyperresponsive

(A) Gross liver morphology of 18-week-old HFD-fed *Fbp1*$^{F/F}$ and *Fbp1*$^{\Delta Hep}$ mice (n = 8–10) that were fasted for 4 h before sacrifice.

(B) H&E, ORO, and PAS staining of liver sections from above mice (n = 8). Scale bars, 20 μm.

(C) ORO and PAS staining intensity per HMF from (B).

(D–G) Serum glucose (D), liver TG (E), serum TG (F), and serum cholesterol (G) in indicated HFD-fed mice (n = 8–10).

(H) Glucose tolerance test (GTT) of HFD-fed *Fbp1*$^{F/F}$ and *Fbp1*$^{\Delta Hep}$ mice (left) (n = 3) and area under the curve (AUC) quantification (right).

(I) Insulin tolerance test (ITT) of HFD-fed *Fbp1*$^{F/F}$ and *Fbp1*$^{\Delta Hep}$ mice (left) (n = 4) and AUC quantification (right).

(J) IB analysis of liver lysates from indicated HFD-fed mice. Densitometric quantification of relative normalized protein ratios (*Fbp1*$^{\Delta Hep}$/*Fbp1*$^{F/F}$), and p values are shown on the right.

(K) IB analysis of liver lysates of HFD-fed 18-week-old *Fbp1*$^{F/F}$ and *Fbp1*$^{\Delta Hep}$ mice collected 15 min after control or insulin injections (n = 4). Quantification of relative normalized protein amounts is shown below each P-AKT strip.

(L) ITT of NCD-fed *Fbp1*$^{F/F}$ and *Fbp1*$^{\Delta Hep}$ mice (top) (n = 4–5) and AUC quantification (bottom).

(M) Human hepatocytes stably transfected with shCtrl or shFBP1 were stimulated with the indicated concentrations of insulin for 1 h after 6 h of serum starvation and IB analyzed with the indicated antibodies.

Data are mean ± SEM. *p < 0.05, **p < 0.01, ***p < 0.001, ****p < 0.0001 (unpaired two-tailed t test).

same fold it has within native FBP1, and is capable of differential association with the N termini of AKT1 and PP2A-C but not with ALDOB (Figures S8E–S8G).

As *FBP1* mRNA is highly expressed in patients with obesity and T2D (GSE15653 and GSE64998) (Figures S8H–S8J), we examined whether FBP1:PP2A-C:ALDOB:AKT complex disruption reverses insulin resistance. We injected the E7 peptide or a scrambled peptide to HFD-fed BL6 mice. Strikingly, the C-terminal peptide disrupted the association of FBP1 with AKT and PP2A-C, and AKT with FBP1, PP2A-C, and ALDOB (Figures 7D and 7E). GST pull-down and PLA confirmed that the FBP1 E7 peptide reduced the association of PP2A-C with FBP1, AKT1, and ALDOB, as well as the AKT-PP2A-C, AKT-FBP1, and FBP1-PP2A-C interactions, but had no effect on the FBP1-ALDOB interaction (Figures 7F and S8K–S8N), which is mediated by FBP1 E1. The E7 peptide enhanced basal and insulin-stimulated AKT activation in HFD-fed WT mice (Figure 7G). *In vitro* dephosphorylation assays showed that the E7 peptide retarded AKT dephosphorylation by PP2A-C (Figure S8O). Importantly, E7 peptide treatment restored glucose tolerance and insulin sensitivity to HFD-fed mice, modestly reducing GNG, lowering their blood glucose, and increasing liver glycogen and lipids with no effect on serum TG, weight gain, or FBP1 catalytic activity (Figures 7H–7J and S8P–S8W). These results establish FBP1 as an important attenuator of insulin signaling in WT mice, suggesting that this non-enzymatic FBP1 function can be exploited in the development of insulin sensitizers for treatment of individuals with obesity-related insulin resistance.

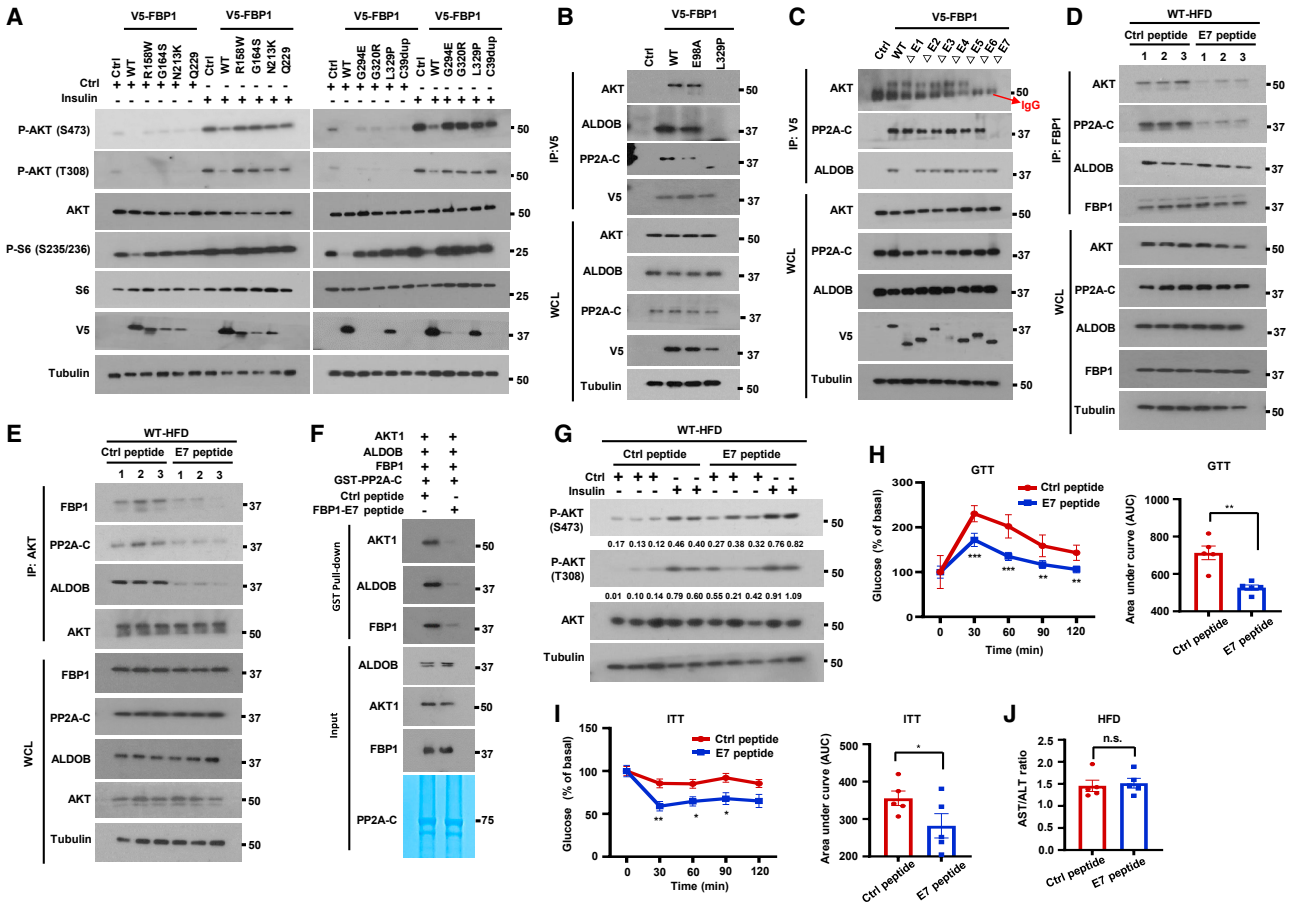

Figure 7. Complex disrupting FBP1-derived C-terminal peptide ameliorates insulin resistance

(A) IB analysis of Huh7 cells stably expressing V5-tagged human FBP1 missense mutants incubated ± insulin (100 nM, 1 h) after 6 h serum starvation.

(B) V5-FBP1, V5-FBP1^{E98A}, and V5-FBP1^{L329P} were IP'ed from stably transfected Huh7 cells, and the gel separated IPs were IB'ed with the indicated antibodies.

(C) To map FBP1 regions interacting with AKT, PP2A-C, and ALDOB, V5-tagged FBP1 exon deletion mutants were stably expressed in Huh7 cells and their association with AKT, PP2A-C, and ALDOB was examined by IP with V5 antibody.

(D and E) Male BL6 mice were placed on HFD for 14 weeks to induce insulin resistance. The mice were injected every other day with Ctrl or FBP1 E7 peptides (10 mg/kg each) for 2 weeks. The mice were then fasted overnight before analysis. Liver lysates were IP'ed with FBP1 (D) or AKT (E) antibodies and AKT, FBP1, and PP2A-C coIPs were IB analyzed.

(F) The GST-PP2A-C pull-down of indicated recombinant proteins was performed in the presence of FBP1 E7 or Ctrl peptides and analyzed as above.

(G) HFD-fed BL6 mice from (D) were injected ± insulin 15 min before being analyzed for liver AKT activation. Relative normalized protein amounts are indicated below the P-AKT strips.

(H) Mice from (D) were fasted overnight and subjected to GTT (n = 5) (left) and AUC quantification (right).

(I) ITT of mice from (D) that were fasted for 2–4 h (n = 5) (I, left) and AUC quantification (I, right).

(J) AST/ALT ratio in mice from (D) (n=5).

Data are presented as mean ± SEM. n.s., not significant, $P \geq 0.05$,*$p < 0.05$, **$p < 0.01$, ***$p < 0.001$ (unpaired two-tailed t test).

DISCUSSION

Until now, the sole metabolic function assigned to FBP1 is the conversion of F1,6-P_2 to F6-P, a critical reaction in GNG.[7,27] In cancer cell nuclei, however, FBP1 was found to inhibit HIF1α activity through protein-protein interactions.[6] Here, we show that cytoplasmic FBP1 has another critical and physiologically relevant metabolic function that does not depend on its enzymatic activity: the formation of a regulatory complex containing PP2A-C and ALDOB that binds AKT and blunts its activation. Discovery of this heretofore unrecognized function, in which FBP1 serves as a safety valve that prevents excessive insulin signaling and balances glucose and lipid metabolism, was enabled by generation of an accurate mouse model of human FBP1 deficiency (OMIM;229700). Similar to FBP1-deficient infants, *Fbp1*$^{\Delta Hep}$ mice, which lack hepatic FBP1 since an early age, are generally normal but exhibit rapid and severe hypoglycemia, hepatomegaly, hepatosteatosis, hyperlipidemia, and liver damage upon fasting. Hypoglycemia and low liver glycogen stores are due to lack of FBP1 catalytic activity, which is needed for GNG and generation of G6-P, the allosteric activator of GYS. By contrast, the different liver pathologies and hyperlipidemia depend on insulin-stimulated AKT hyperactivation and not on FBP1 catalytic activity. Accordingly, these pathologies, but not hypoglycemia, are prevented by re-expression of catalytically inactive FBP1, inhibition of AKT, and, to a lesser extent, by

inhibition of mTORC1. In addition to stimulation of protein synthesis,[28] a likely driver of hepatomegaly, mTORC1 activates the lipogenic transcription factor SREBP1c,[14] accounting for increased lipogenesis and hyperlipidemia. Enhanced AKT activation may also contribute to some of the long-term metabolic abnormalities seen in older FBP1 deficient individuals.[8] A somewhat different phenotype that includes liver damage, fibrosis, and enhanced hepatocyte tumorigenesis, but little or no effect on glucose tolerance, was observed after AAV-Cre-mediated FBP1 ablation in older (24-week-old) *Fbp1*$^{F/F}$ mice.[11] These phenotypic differences are most likely due to the timing of FBP1 ablation and the evaluation of glucose tolerance in lean vs. HFD-fed mice.

Although it causes AKT hyperactivation in fasted and insulin-treated mice, hepatocyte FBP1 deficiency protects HFD-fed mice from glucose intolerance. The catalytically inactive FBP1^{E98A} variant binds ALDOB and PP2A-C and inhibits AKT activation as effectively as the native protein, but human *FBP1* missense mutants that are not severely destabilized, L329P, R158W, G164S, and N213K, are devoid of AKT inhibitory activity. One of the residues affected by these mutations, L329, is not a part of the catalytic pocket[29,30] and is associated with only a modest decrease in FBPase activity, underscoring the disconnect between loss of GNG and insulin hyperresponsiveness. MS, IP, gel filtration, and PLA demonstrated that FBP1 is the lynchpin responsible for formation of the FBP1:PP2A-C:ALDOB:AKT regulatory complex. Although insulin destabilizes this complex to facilitate AKT activation, HFD stimulates FBP1 expression and complex formation, suggesting that elevated FBP1 expression is a previously unknown contributor to HFD-induced insulin resistance. Although more precise understanding of the interactions between FBP1, AKT, PP2A-C, and ALDOB requires detailed structural analysis, our biochemical analysis suggests that the regulatory function of FBP1 depends on the recruitment of PP2A-C to AKT, rather than other phosphoproteins. Of note, a synthetic peptide derived from *FBP1* E7 can be docked onto AKT and PP2A-C and disrupt their interactions with native FBP1. By potentiating AKT activation, this peptide serves as an insulin mimic, capable of reversing obesity-induced glucose intolerance, and further demonstrating the physiological relevance of the FBP1 nucleated AKT inhibitory complex. Although, similar to insulin secretagogues and sensitizers, E7 treatment modestly potentiates hepatosteatosis, the restoration of insulin sensitivity outweighs the increased risk of hepatosteatosis, which could be circumvented by co-treatment with β-oxidation-inducing uncouplers.[31] The non-enzymatic regulatory function of FBP1 probably appeared early in vertebrate evolution, as it modulates liver energy storage and lipid production, which are highly important in egg laying animals. In addition to causing potentially fatal insulin hyperresponsiveness, the loss of FBP1 regulatory function may also increase the risk of non-alcoholic steatohepatitis.

Limitations of study

Our study indicates that FBP1 inhibits insulin hyperresponsiveness by promoting assembly of the FBP1:PP2A-C:ALDOB:AKT regulatory complex, which can be reconstituted using purified proteins. However, we cannot rule out the existence of additional constituents that modulate complex assembly and stability. We have used FBP1 ablation to demonstrate the importance of its AKT-regulating function in mice and human hepatocytes, but because of the absence of human clinical specimens, we did not demonstrate that the human FBP1 deficiency also results in AKT hyperactivation. The E7 peptide reverses insulin resistance by disrupting the FBP1:PP2A-C:ALDOB:AKT complex, but further sequence optimization may create more potent E7 variants, which will ameliorate insulin resistance at a lower dose. Clinical trials will be needed for establishing the human efficacy of such peptides and determine whether they can reverse insulin resistance without further aggravation of hepatosteatosis.

STAR★METHODS

Detailed methods are provided in the online version of this paper and include the following:

- KEY RESOURCES TABLE
- RESOURCE AVAILABILITY
  - Lead contact
  - Materials availability
  - Data and code availability
- EXPERIMENTAL MODEL AND SUBJECT DETAILS
  - Mice
  - Cell Culture and Reagents
  - Human hepatocytes
- METHOD DETAILS
  - Constructs
  - Plasmid transfection and virus infection
  - Immunoblot analysis and nuclear extraction
  - Histology
  - Measurements of metabolites and hormones
  - [U-^{13}C] glucose, ^{13}C-lactate and D_2O labeling
  - Stable-Isotope Tracer Metabolomics
  - Size Exclusion Chromatography
  - FBP1 activity assay
  - GTT, PTT, and ITT
  - Glycogen extraction
  - Glycogen Synthase Activity
  - Measuring liver protein synthesis with O-propargyl-puromycin
  - Generation and infection by AAV8-FBP1, AAV8-FBP1^{E98A} and AAV8-Ctrl virus
  - Primary mouse hepatocytes isolation
  - Proximity ligation assays (PLA)
  - Immunoprecipitation and mass spectrometry analysis
  - In vitro binding assay
  - PP2A dephosphorylation assay
  - Peptide synthesis and treatment
  - Protein structure predictions and peptide docking
  - RNA isolation and quantitative real-time PCR (Q-PCR)
- QUANTIFICATION AND STATISTICAL ANALYSIS

SUPPLEMENTAL INFORMATION

Supplemental information can be found online at https://doi.org/10.1016/j.cmet.2023.03.021.

ACKNOWLEDGMENTS

We thank the Karin Lab for helpful discussions and Cell Signaling Technologies, Santa Cruz Technologies, and Life Technologies for gifts of antibodies/other reagents, the UCSD histology core for assistance, Sanford Burnham Prebys Cancer Metabolism Core for the metabolomic analyses, and Collaborative Center for multiplexed proteomics at UCSD. Funding: research was supported by NIH grants to M.K. (R01DK120714 and R01CA234128), M.K. and J.H.L. (R01DK133448), M.C.S. (P01CA104838 and R35CA197602), A.R.S. (R01DK117551, R01DK125820, R01DK076906, and P30DK063491), W.Y. (R21HD107516, R00DK115998, and R01DK125560), and A.C.N. (R35 GM122523). M.K. hold the Ben and Wanda Hildyard Chair for Mitochondrial and Metabolic Diseases and is an American Cancer Society Research Professor. A.C.J. was supported in part by the University of California, San Diego, Graduate Training Program in Cellular and Molecular Pharmacology (T32 GM007752) and the National Science Foundation Graduate Research Fellowship (#DGE-1650112).

AUTHOR CONTRIBUTIONS

M.K. and L.G. conceived the project. L.G. and Y.Z. designed the study and performed most of the experiments. K.W., M.L., J.L., S.P., M.T., F.L., K.C.R., and A.C.J assisted with experiments and data analysis. J.E.M. assisted with gel filtration analysis. B.Z. performed glycogen content analysis and GYS2 IB. L.C.K selected and provided the $FBP1^{E98A}$ variant. X.L. and T.K. provided human hepatocytes. J.H.L. performed Seq-Scope analysis. I.H.W. and D.J.G. performed the mass spectrometry. W.Y., A.C.N., A.R.S., and M.C.S. provided important reagents, advice, and helped with data interpretation and discussion. M.K. and L.G. wrote the manuscript, with all authors contributing and proving feedback and advice.

DECLARATION OF INTERESTS

M.K. and A.R.S. are founders and stockholders in Elgia Pharmaceuticals, and M.K. had received research support from Merck and Janssen Pharmaceuticals.

Received: November 29, 2022
Revised: February 16, 2023
Accepted: March 30, 2023
Published: April 20, 2023

REFERENCES

1. Saltiel, A.R. (2021). Insulin signaling in health and disease. J. Clin. Invest. *131*. https://doi.org/10.1172/JCI142241.
2. Petersen, M.C., Vatner, D.F., and Shulman, G.I. (2017). Regulation of hepatic glucose metabolism in health and disease. Nat. Rev. Endocrinol. *13*, 572–587. https://doi.org/10.1038/nrendo.2017.80.
3. Hatting, M., Tavares, C.D.J., Sharabi, K., Rines, A.K., and Puigserver, P. (2018). Insulin regulation of gluconeogenesis. Ann. NY Acad. Sci. *1411*, 21–35. https://doi.org/10.1111/nyas.13435.
4. Santoleri, D., and Titchenell, P.M. (2019). Resolving the paradox of hepatic insulin resistance. Cell. Mol. Gastroenterol. Hepatol. *7*, 447–456. https://doi.org/10.1016/j.jcmgh.2018.10.016.
5. Hay, N. (2011). Interplay between FOXO, TOR, and Akt. Biochim. Biophys. Acta *1813*, 1965–1970. https://doi.org/10.1016/j.bbamcr.2011.03.013.
6. Li, B., Qiu, B., Lee, D.S., Walton, Z.E., Ochocki, J.D., Mathew, L.K., Mancuso, A., Gade, T.P., Keith, B., Nissim, I., and Simon, M.C. (2014). Fructose-1,6-bisphosphatase opposes renal carcinoma progression. Nature *513*, 251–255. https://doi.org/10.1038/nature13557.
7. Hunter, R.W., Hughey, C.C., Lantier, L., Sundelin, E.I., Peggie, M., Zeqiraj, E., Sicheri, F., Jessen, N., Wasserman, D.H., and Sakamoto, K. (2018). Metformin reduces liver glucose production by inhibition of fructose-1-6-bisphosphatase. Nat. Med. *24*, 1395–1406. https://doi.org/10.1038/s41591-018-0159-7.
8. Gorce, M., Lebigot, E., Arion, A., Brassier, A., Cano, A., De Lonlay, P., Feillet, F., Gay, C., Labarthe, F., Nassogne, M.C., et al. (2022). Fructose-1,6-bisphosphatase deficiency causes fatty liver disease and requires long-term hepatic follow-up. J. Inherit. Metab. Dis. *45*, 215–222. https://doi.org/10.1002/jimd.12452.
9. Salih, R.M., Mohammed, E.A., Alhashem, A.M., Mohamed, S., and Al-Aqeel, A.I. (2020). Fructose-1,6-bisphosphatase deficiency with confirmed molecular diagnosis. An important cause of hypoglycemia in children. Saudi Med. J. *41*, 199–202. https://doi.org/10.15537/smj.2020.2.24885.
10. Moey, L.H., Abdul Azize, N.A., Yakob, Y., Leong, H.Y., Keng, W.T., Chen, B.C., and Ngu, L.H. (2018). Fructose-1,6-bisphosphatase deficiency as a cause of recurrent hypoglycemia and metabolic acidosis: clinical and molecular findings in Malaysian patients. Pediatr. Neonatol. *59*, 397–403. https://doi.org/10.1016/j.pedneo.2017.11.006.
11. Li, F., Huangyang, P., Burrows, M., Guo, K., Riscal, R., Godfrey, J., Lee, K.E., Lin, N., Lee, P., Blair, I.A., et al. (2020). FBP1 loss disrupts liver metabolism and promotes tumorigenesis through a hepatic stellate cell senescence secretome. Nat. Cell Biol. *22*, 728–739. https://doi.org/10.1038/s41556-020-0511-2.
12. Schultze, S.M., Hemmings, B.A., Niessen, M., and Tschopp, O. (2012). PI3K/AKT, MAPK and AMPK signalling: protein kinases in glucose homeostasis. Expert Rev. Mol. Med. *14*, e1. https://doi.org/10.1017/S1462399411002109.
13. Grill, V., and Qvigstad, E. (2000). Fatty acids and insulin secretion. Br. J. Nutr. *83*, S79–S84. https://doi.org/10.1017/s0007114500000994.
14. Bakan, I., and Laplante, M. (2012). Connecting mTORC1 signaling to SREBP-1 activation. Curr. Opin. Lipidol. *23*, 226–234. https://doi.org/10.1097/MOL.0b013e328352dd03.
15. Benhamed, F., Denechaud, P.D., Lemoine, M., Robichon, C., Moldes, M., Bertrand-Michel, J., Ratziu, V., Serfaty, L., Housset, C., Capeau, J., et al. (2012). The lipogenic transcription factor ChREBP dissociates hepatic steatosis from insulin resistance in mice and humans. J. Clin. Invest. *122*, 2176–2194. https://doi.org/10.1172/JCI41636.
16. Beurel, E., Grieco, S.F., and Jope, R.S. (2015). Glycogen synthase kinase-3 (GSK3): regulation, actions, and diseases. Pharmacol. Ther. *148*, 114–131. https://doi.org/10.1016/j.pharmthera.2014.11.016.
17. Villar-Palasí, C., and Guinovart, J.J. (1997). The role of glucose 6-phosphate in the control of glycogen synthase. FASEB J. *11*, 544–558.
18. Herman, M.A., and Birnbaum, M.J. (2021). Molecular aspects of fructose metabolism and metabolic disease. Cell Metab. *33*, 2329–2354. https://doi.org/10.1016/j.cmet.2021.09.010.
19. Simons, N., Debray, F.G., Schaper, N.C., Kooi, M.E., Feskens, E.J.M., Hollak, C.E.M., Lindeboom, L., Koek, G.H., Bons, J.A.P., Lefeber, D.J., et al. (2019). Patients with aldolase B deficiency are characterized by increased intrahepatic triglyceride content. J. Clin. Endocrinol. Metab. *104*, 5056–5064. https://doi.org/10.1210/jc.2018-02795.
20. Oppelt, S.A., Sennott, E.M., and Tolan, D.R. (2015). Aldolase-B knockout in mice phenocopies hereditary fructose intolerance in humans. Mol. Genet. Metab. *114*, 445–450. https://doi.org/10.1016/j.ymgme.2015.01.001.
21. Di Dato, F., Spadarella, S., Puoti, M.G., Caprio, M.G., Pagliardini, S., Zuppaldi, C., Vallone, G., Fecarotta, S., Esposito, G., Iorio, R., et al. (2019). Daily fructose traces intake and liver injury in children with hereditary fructose intolerance. Nutrients *11*, 2397. https://doi.org/10.3390/nu11102397.
22. Droppelmann, C.A., Sáez, D.E., Asenjo, J.L., Yáñez, A.J., García-Rocha, M., Concha, I.I., Grez, M., Guinovart, J.J., and Slebe, J.C. (2015). A new level of regulation in gluconeogenesis: metabolic state modulates the intracellular localization of aldolase B and its interaction with liver fructose-1,6-bisphosphatase. Biochem. J. *472*, 225–237. https://doi.org/10.1042/BJ20150269.
23. He, X., Li, M., Yu, H., Liu, G., Wang, N., Yin, C., Tu, Q., Narla, G., Tao, Y., Cheng, S., and Yin, H. (2020). Loss of hepatic aldolase B activates Akt and promotes hepatocellular carcinogenesis by destabilizing the

Aldob/Akt/PP2A protein complex. PLoS Biol. *18*, e3000803. https://doi.org/10.1371/journal.pbio.3000803.

24. Crespin, S.R., Greenough, W.B., 3rd, and Steinberg, D. (1969). Stimulation of insulin secretion by infusion of free fatty acids. J. Clin. Invest. *48*, 1934–1943. https://doi.org/10.1172/JCI106160.
25. Graham, M.L., Janecek, J.L., Kittredge, J.A., Hering, B.J., and Schuurman, H.J. (2011). The streptozotocin-induced diabetic nude mouse model: differences between animals from different sources. Comp. Med. *61*, 356–360.
26. Emecen Sanli, M., Cengiz, B., Kilic, A., Ozsaydi, E., Inci, A., Okur, I., Tumer, L., Lebigot, E., and Ezgu, F. (2022). Fructose 1,6 bisphosphatase deficiency: outcomes of patients in a single center in Turkey and identification of novel splice site and indel mutations in FBP1. J. Pediatr. Endocrinol. Metab. *35*, 497–503. https://doi.org/10.1515/jpem-2021-0732.
27. Leithner, K. (2020). Epigenetic marks repressing gluconeogenesis in liver and kidney cancer. Cancer Res. *80*, 657–658. https://doi.org/10.1158/0008-5472.CAN-19-3953.
28. Bhaskar, P.T., and Hay, N. (2007). The two TORCs and Akt. Dev. Cell *12*, 487–502. https://doi.org/10.1016/j.devcel.2007.03.020.
29. Ruf, A., Tetaz, T., Schott, B., Joseph, C., and Rudolph, M.G. (2016). Quadruple space-group ambiguity owing to rotational and translational noncrystallographic symmetry in human liver fructose-1,6-bisphosphatase. Acta Crystallogr. D Struct. Biol. *72*, 1212–1224. https://doi.org/10.1107/S2059798316016715.
30. Huang, Y., Xu, Y., Song, R., Ni, S., Liu, J., Xu, Y., Ren, Y., Rao, L., Wang, Y., Wei, L., et al. (2020). Identification of the new covalent allosteric Binding Site of fructose-1,6-bisphosphatase with disulfiram derivatives toward glucose reduction. J. Med. Chem. *63*, 6238–6247. https://doi.org/10.1021/acs.jmedchem.0c00699.
31. Goedeke, L., Peng, L., Montalvo-Romeral, V., Butrico, G.M., Dufour, S., Zhang, X.M., Perry, R.J., Cline, G.W., Kievit, P., Chng, K., et al. (2019). Controlled-release mitochondrial protonophore (CRMP) reverses dyslipidemia and hepatic steatosis in dysmetabolic nonhuman primates. Sci. Transl. Med. *11*. https://doi.org/10.1126/scitranslmed.aay0284.
32. He, F., Antonucci, L., Yamachika, S., Zhang, Z., Taniguchi, K., Umemura, A., Hatzivassiliou, G., Roose-Girma, M., Reina-Campos, M., Duran, A., et al. (2020). NRF2 activates growth factor genes and downstream AKT signaling to induce mouse and human hepatomegaly. Journal of hepatology *72*, 1182–1195. https://doi.org/10.1016/j.jhep.2020.01.023.
33. Kim, J.Y., Garcia-Carbonell, R., Yamachika, S., Zhao, P., Dhar, D., Loomba, R., Kaufman, R.J., Saltiel, A.R., and Karin, M. (2018). ER stress drives lipogenesis and steatohepatitis via caspase-2 activation of S1P. Cell *175*. 133.e15-145.e15. https://doi.org/10.1016/j.cell.2018.08.020.
34. Todoric, J., Di Caro, G., Reibe, S., Henstridge, D.C., Green, C.R., Vrbanac, A., Ceteci, F., Conche, C., McNulty, R., Shalapour, S., et al. (2020). Fructose stimulated de novo lipogenesis is promoted by inflammation. Nat. Metab. *2*, 1034–1045. https://doi.org/10.1038/s42255-020-0261-2.
35. Gu, L., Zhu, Y., Lin, X., Lu, B., Zhou, X., Zhou, F., Zhao, Q., Prochownik, E.V., and Li, Y. (2021). The IKKβ-USP30-ACLY axis controls lipogenesis and tumorigenesis. Hepatology *73*, 160–174. https://doi.org/10.1002/hep.31249.
36. Zwingmann, C., and Bilodeau, M. (2006). Metabolic insights into the hepatoprotective role of N-acetylcysteine in mouse liver. Hepatology *43*, 454–463. https://doi.org/10.1002/hep.21075.
37. SenGupta, A., Ghosh, S., Sharma, S., and Sonawat, H.M. (2020). Early perturbations in glucose utilization in malaria-infected murine erythrocytes, liver and brain observed by metabolomics. Metabolites *10*, 277. https://doi.org/10.3390/metabo10070277.
38. Gray, L.R., Sultana, M.R., Rauckhorst, A.J., Oonthonpan, L., Tompkins, S.C., Sharma, A., Fu, X., Miao, R., Pewa, A.D., Brown, K.S., et al. (2015). Hepatic mitochondrial pyruvate Carrier 1 is required for efficient regulation of gluconeogenesis and whole-body glucose homeostasis. Cell Metab. *22*, 669–681. https://doi.org/10.1016/j.cmet.2015.07.027.
39. Huh, J.Y., Reilly, S.M., Abu-Odeh, M., Murphy, A.N., Mahata, S.K., Zhang, J., Cho, Y., Seo, J.B., Hung, C.W., Green, C.R., et al. (2020). TANK-binding kinase 1 regulates the localization of acyl-CoA synthetase ACSL1 to control hepatic fatty acid oxidation. Cell Metab. *32*. 1012.e7-1027.e7. https://doi.org/10.1016/j.cmet.2020.10.010.
40. Scott, D.A. (2021). Analysis of melanoma cell glutamine metabolism by stable isotope tracing and gas chromatography-mass spectrometry. Methods Mol. Biol. *2265*, 91–110. https://doi.org/10.1007/978-1-0716-1205-7_7.
41. Bouskila, M., Hunter, R.W., Ibrahim, A.F., Delattre, L., Peggie, M., van Diepen, J.A., Voshol, P.J., Jensen, J., and Sakamoto, K. (2010). Allosteric regulation of glycogen synthase controls glycogen synthesis in muscle. Cell Metab. *12*, 456–466. https://doi.org/10.1016/j.cmet.2010.10.006.
42. Liu, J., Xu, Y., Stoleru, D., and Salic, A. (2012). Imaging protein synthesis in cells and tissues with an alkyne analog of puromycin. Proc. Natl. Acad. Sci. USA *109*, 413–418. https://doi.org/10.1073/pnas.1111561108.
43. He, F., Antonucci, L., Yamachika, S., Zhang, Z., Taniguchi, K., Umemura, A., Hatzivassiliou, G., Roose-Girma, M., Reina-Campos, M., Duran, A., et al. (2020). NRF2 activates growth factor genes and downstream AKT signaling to induce mouse and human hepatomegaly. J. Hepatol. *72*, 1182–1195. https://doi.org/10.1016/j.jhep.2020.01.023.
44. Su, H., Yang, F., Fu, R., Li, X., French, R., Mose, E., Pu, X., Trinh, B., Kumar, A., Liu, J., et al. (2021). Cancer cells escape autophagy inhibition via NRF2-induced macropinocytosis. Cancer Cell *39*. 678.e11-693.e11. https://doi.org/10.1016/j.ccell.2021.02.016.
45. Jumper, J., Evans, R., Pritzel, A., Green, T., Figurnov, M., Ronneberger, O., Tunyasuvunakool, K., Bates, R., Žídek, A., Potapenko, A., et al. (2021). Highly accurate protein structure prediction with AlphaFold. Nature *596*, 583–589. https://doi.org/10.1038/s41586-021-03819-2.

Please cite this article in press as: Gu et al., Fructose-1,6-bisphosphatase is a nonenzymatic safety valve that curtails AKT activation to prevent insulin hyperresponsiveness, Cell Metabolism (2023), https://doi.org/10.1016/j.cmet.2023.03.021

STAR★METHODS

KEY RESOURCES TABLE

REAGENT or RESOURCE	SOURCE	IDENTIFIER
Antibodies		
Rabbit polyclonal anti-FBP1	Sigma	Cat# HPA005857; RRID:AB_1848445
Rabbit monoclonal anti-FBP1	Abcam	Cat# ab109020; RRID:AB_10865049
Rabbit polyclonal anti-AKT	Cell Signaling	Cat# 9272; RRID:AB_329827
Mouse monoclonal anti-AKT	Cell Signaling	Cat# 2920; RRID:AB_1147620
Rabbit monoclonal anti-AKT1	Cell Signaling	Cat# 2938; RRID:AB_915788
Rabbit monoclonal anti-AKT2	Cell Signaling	Cat# 3063; RRID: AB_2225186
Rabbit polyclonal anti-P-AKT (S473)	Cell Signaling	Cat# 9271; RRID:AB_329825
Rabbit monoclonal anti-P-AKT (T308)	Cell Signaling	Cat# 4056; RRID:AB_331163
Rabbit polyclonal anti-ALDOB	Proteintech	Cat# 18065-1-AP; RRID:AB_2273968
Mouse monoclonal anti-ALDOB	Santa Cruze	Cat# sc-393278
Mouse monoclonal anti-Tubulin	Sigma	Cat# T9026; RRID:AB_477593
Rabbit monoclonal anti-GSK3β	Cell Signaling	Cat# 12456; RRID:AB_2636978
Rabbit monoclonal anti-P-GSK3β	Cell Signaling	Cat# 9323; RRID:AB_2115201
Rat monoclonal anti-HA	Sigma	Cat# 1867431
Mouse monoclonal anti-V5	Invitrogen	Cat# R960-25; RRID:AB_2556564
Mouse monoclonal anti-PP2A-C	Sigma	Cat# 05-421; RRID:AB_309726
Rabbit Polyclonal anti-PP2A-C	Cell Signaling	Cat# 2038; RRID:AB_2169495
Mouse monoclonal anti-Flag	Sigma	Cat# F3165; RRID:AB_259529
Mouse monoclonal anti-S6	Cell Signaling	Cat# 2317; RRID:AB_2238583
Rabbit monoclonal anti-P-S6(S235/236)	Cell Signaling	Cat# 4858; RRID:AB_916156
Rabbit polyclonal anti-AMPK	Santa Cruz	Cat# sc-25792; RRID:AB_2169546
Rabbit monoclonal anti-P-AMPK(Thr172)	Cell Signaling	Cat# 2535; RRID:AB_331250
Mouse monoclonal anti-P70S6K	Santa Cruz	Cat# sc-8418; RRID:AB_628094
Mouse monoclonal anti-P-P70S6K(T389)	Cell Signaling	Cat# 9206; RRID:AB_2285392
Mouse monoclonal anti-Myc	Sigma	Cat# 05-724; RRID:AB_309938
Goat anti-Rabbit IgG (H+L) Highly Cross-Adsorbed Secondary Antibody, Alexa Fluor Plus 488	Thermo Fisher Scientific	Cat# A32731; RRID:AB_2633280
Goat anti-Mouse IgG (H+L) Highly Cross-Adsorbed Secondary Antibody, Alexa Fluor Plus 488	Thermo Fisher Scientific	Cat#A32723; RRID: AB_2633275
Goat anti-Rabbit IgG (H+L) Highly Cross-Adsorbed Secondary Antibody, Alexa Fluor Plus 594	Thermo Fisher Scientific	Cat# A32740; RRID:AB_2762824
Goat anti-Mouse IgG (H+L) Highly Cross-Adsorbed Secondary Antibody, Alexa Fluor 568	Thermo Fisher Scientific	Cat#A-11031; RRID:AB_144696
Mouse monoclonal anti-SREBP1	Abcam	Cat# ab3259; RRID:AB_303650
Rabbit polyclonal anti-Histone H3	ABclonal	Cat# A2348; RRID:AB_2631273
Rabbit polyclonal anti-ACLY	Cell Signaling	Cat# 4332; RRID:AB_2223744
Rabbit monoclonal anti-FASN	Cell Signaling	Cat# 3180; RRID:AB_2100796

(*Continued on next page*)

Please cite this article in press as: Gu et al., Fructose-1,6-bisphosphatase is a nonenzymatic safety valve that curtails AKT activation to prevent insulin hyperresponsiveness, Cell Metabolism (2023), https://doi.org/10.1016/j.cmet.2023.03.021

Continued

REAGENT or RESOURCE	SOURCE	IDENTIFIER
Rabbit Polyclonal anti-ATGL	Cell Signaling	Cat# 2138; RRID:AB_2167955
Rabbit polyclonal anti-P-ATGL(S406)	Abcam	Cat# Ab135093; RRID:AB_2888660
Rabbit polyclonal anti-HSL	Santa Cruz	Cat# sc-25843; RRID:AB_2135501
Rabbit polyclonal anti-P-HSL(S660)	Cell Signaling	Cat# 4126; RRID:AB_490997
Rabbit polyclonal anti-P-HSL(S565)	Cell Signaling	Cat# 4137; RRID:AB_2135498
Rabbit polyclonal anti-CHREBP	Novus Biologicals	Cat# NB400-135; RRID:AB_10002435
Rabbit monoclonal anti-GR	Cell Signaling	Cat# 12041; RRID:AB_2631286
Rabbit monoclonal anti-P-GYS2	Cell Signaling	Cat# 47043; RRID:AB_2799317
Rabbit polyclonal anti-GYS2	Proteintech	Cat# 22371-1; RRID:AB_2879091
Mouse monocolonal anti-Myc	Upstate	Cat# 05-724; RRID:AB_309938
Rabbit monocolonal anti-P-c-Myc (S62)	Cell Signaling	Cat# 13748; RRID:AB_2687518
Mouse monoclonal anti-GST	BD Biosciences	Cat# 554805; RRID:AB_395536
Chemicals and Reagent		
MK2206	MCE	HY-10358
Torin1	MCE	HY-13003
Streptozotocin	Sigma	S0130
Cycloheximide	Sigma	CHX; C7698
Insulin	Sigma	11061-68-0
FBP1	Prospec	ENZ-454
AKT1	Prospec	PKA-068
ALDOB	Prospec	ENZ-245
GST-PP2A-C	BPS Bioscience	30056
GST-PP2A-C	LSBio	LS-G29851
Dynabeads™ Protein A for Immunoprecipitation	Thermo Fisher	10008D
Dynabeads™ Protein G for Immunoprecipitation	Thermo Fisher	10009D
D-glucose (U-13C6, 99%)	Cambridge Isotope Laboratories	NC9337143
13C-lactate	Cambridge Isotope Laboratories	CLM-1579
Deuterium oxide	Sigma	151882
UDP-glucose	Sigma	U4625
Glucose-6-phosphate	Sigma	10127647001
Glycogen	Sigma	G0885
Percoll	GE healthcare	10226958
Liberase™ TM Research Grade	Sigma	5401127001
Cultrex Rat Collagen I	R&D systems	3440-100-01
Polybrene	Santa Cruze	sc-134220
Puromycin	IntivoGen	ant-pr-1
Lipofectamine 300 Transfection Reagent	Thermo Fisher	L3000015
O-propargyl-puromycin	MedChemExpress	HY-15680
Critical Commercial Assays		
PAS kit	Thermo Fisher	#87007
Lipofectamine 3000	Invitrogen	L300008
NE-PER™ Nuclear and Cytoplasmic Extraction Reagent kit	Thermo Fisher	78833
Insulin ELISA KIT	Invitrogen	EMMINS

(*Continued on next page*)

Please cite this article in press as: Gu et al., Fructose-1,6-bisphosphatase is a nonenzymatic safety valve that curtails AKT activation to prevent insulin hyperresponsiveness, Cell Metabolism (2023), https://doi.org/10.1016/j.cmet.2023.03.021

Continued

REAGENT or RESOURCE	SOURCE	IDENTIFIER
Glucagon ELISA KIT	Invitrogen	EMMINS
NADP/NADPH-GloTM Assays	Promega	#G9081
ALT(GPT) Reagent	Thermo Scientific™	TR71121
AST/GOT Reagent	Thermo Scientific™	TR70121
ATP assay kit	Abcam	ab83355
Acetyl-Coenzyme A Assay Kit	Sigma	MAK039
PicoProbe™ Glucose-6-Phosphate Fluorometric Assay Kit	Biovision	K687
Glucose colorimetric assay kit	Cayman Chemical	#10009582
Lactate Colorimetric/Fluorometric Assay Kit	Biovision	K607
Superdex 200 HR 10/30 column	Pharmacia Biotech	Cat # 17-1088-01
Fructose-1,6-Bisphosphatase Activity Assay Kit (Colorimetric)	Abcam	ab273329
Fujifilm Autokit glucose assay	Fujifilm Autokit	997-03001
Click-&-Go Plus 488 OPP Protein Synthesis Assay Kit	Click Chemistry	# 1493
Duolink® In Situ Red Starter Kit Mouse/Rabbit	Sigma	DUO92101
Transcreener UDP^2 FI assay	BellBrook	3019-A
RNeasy Plus Mini kit	Qiagen	#74134
SuperScript™ VILO™ cDNA Synthesis Kit	Thermo Fisher	11754050
Deposited data		
Source data for all figures	This paper	Data S1
Experimental Models: Cell Lines		
Huh7	N/A	N/A
HepG2	ATCC	ATCCHB-8065
HK-2	Dr. M. Celeste Simon	N/A
Caco-2	ATCC	HTB-37
293T	ATCC	CRL-3216
Experimental Models: Organisms/Strains		
Fbp1F/F	Dr. M. Celeste Simon	N/A
Alb-Cre	He et al., 2020a[32]	N/A
Recombinant DNA		
FBP1-R158W	This paper	N/A
FBP1-G164S	This paper	N/A
FBP1-N213K	This paper	N/A
FBP1-Q229	This paper	N/A
FBP1-G294E	This paper	N/A
FBP1-G320R	This paper	N/A
FBP1-L329P	This paper	N/A
FBP1-C39dup	This paper	N/A
FBP1-S321A	This paper	N/A
V5-FBP1	Dr. M. Celeste Simon	N/A
V5-FBP1 E98A	Dr. M. Celeste Simon	N/A
FBP1-ΔE1	Dr. M. Celeste Simon	N/A
FBP1-ΔE2	Dr. M. Celeste Simon	N/A
FBP1-ΔE3	Dr. M. Celeste Simon	N/A
FBP1-ΔE4	Dr. M. Celeste Simon	N/A
FBP1-ΔE5	Dr. M. Celeste Simon	N/A

(*Continued on next page*)

Please cite this article in press as: Gu et al., Fructose-1,6-bisphosphatase is a nonenzymatic safety valve that curtails AKT activation to prevent insulin hyperresponsiveness, Cell Metabolism (2023), https://doi.org/10.1016/j.cmet.2023.03.021

Continued

REAGENT or RESOURCE	SOURCE	IDENTIFIER
FBP1-ΔE6	Dr. M. Celeste Simon	N/A
FBP1-ΔE7	Dr. M. Celeste Simon	N/A
Oligonucleotides		
Primer sequence for constructs, See Table S1	This paper	N/A
shRNAs targeting sequence, see Table S2	This paper	N/A
See Table S3 for qPCR primer list	This paper	N/A
Software		
ImageJ	NIH	https://imagej.nih.gov/ij/
Graphpad Prism 7	Graphpad	https://www.graphpad.com/scientificsoftware/prism/

RESOURCE AVAILABILITY

Lead contact

Further information and requests for resources and reagents should be directed to and will be fulfilled by the lead contact, Michael Karin (karinoffice@ucsd.edu).

Materials availability

All unique/stable reagents generated in this study are available from the lead contact without restriction.

Data and code availability

- All data reported in this paper will be shared by the lead contact upon request. Uncropped western blots and source data related to Figures 1, 2, 3, 4, 5, 6, 7, and S1–S8 can be found in Data S1.
- This paper does not report original codes.
- Any additional information required to reanalyze the data reported in this paper is available from the lead contact upon request.

EXPERIMENTAL MODEL AND SUBJECT DETAILS

Mice

Fbp1$^{F/F}$ mice were generated by Dr. M. Celeste Simon (University of Pennsylvania, Philadelphia)[11] and crossed to *Alb-Cre* mice to generate *Fbp1*$^{\Delta Hep}$ mice at UCSD. All mice were backcrossed into the BL6 background at least nine generations, and only male mice were used in most experiments. Mice were maintained in filter-topped cages on autoclaved food and water with a 12 h light (6am-6pm)/ dark (6pm-6am) cycle. Experiments were performed according to UCSD Institutional Animal Care and Use Committee and NIH guidelines and regulations. Dr. Karin's Animal protocol S00218 was approved by the UCSD Institutional Animal Care and Use Committee. Where indicated, mice were fed with HFD (#S3282, Bio-serv) for a total of 12 wk, starting at 7 wk-of-age. Body weight and food consumption were monitored bi-weekly throughout the entire feeding period.[33] Mice were starved for 4 h or 16 h before blood collection and sacrifice and liver and adipose tissue were excised and weighed. Where indicated, male *Fbp1*$^{F/F}$ and *Fbp1*$^{\Delta Hep}$ mice (8 wo) were intraperitoneally (i.p.) injected with MK2206 (100 mg/kg) or Torin1 (10 mg/kg) on 2 sequential days prior to fasting from 6 pm to 10 am, at which point the mice were euthanized for blood and tissue collection. The number of mice per experiment and their ages are indicated in the figure legends.

For streptozotocin treatment, 8-10 wo *Fbp1*$^{F/F}$ and *Fbp1*$^{\Delta Hep}$ male and female mice were i.p. injected with 150 mg/kg STZ. Mice were monitored daily for food and water consumption. Blood glucose was measured daily at random. After 5-7 days, mice with substantial hyperglycemia were fasted for 4 h before euthanasia and liver and blood analyses.

Cell Culture and Reagents

Human HCC HepG2 and Huh7 cell lines were purchased from ATCC (HB-8065) and Cell bank, respectively. Huh7, HepG2, Caco-2 and 293T cells were tested regularly to confirm they are mycoplasma negative, and cultured in low glucose DMEM (Life technologies, 11885084), MEM (Life technologies, 11095080, and DMEM (Life technologies, 2366044), respectively, plus 10% fetal bovine serum (FBS) (Gibco), penicillin (100 mg/ml) and streptomycin (100 mg/ml). The HK-2 kidney cell line was provided by Dr. Celeste Simon and cultured in Keratinocyte-SFM medium supplemented with human recombinant epidermal growth factor (EGF) and bovine pituitary extract (BPE) (Life Technologies).6 Cells were incubated at 37°C in a humidified chamber with 5% CO2. Cells were treated with insulin (Sigma 11061-68-0) at the times and concentrations indicated in figure legends.

Please cite this article in press as: Gu et al., Fructose-1,6-bisphosphatase is a nonenzymatic safety valve that curtails AKT activation to prevent insulin hyperresponsiveness, Cell Metabolism (2023), https://doi.org/10.1016/j.cmet.2023.03.021

Human hepatocytes

Donor livers rejected for transplantation were obtained via Lifesharing OPO as a part of T. Kisseleva's research program. Donors, who had no history of alcohol abuse, body- mass index 33.82, had no liver fibrosis and minimal liver steatosis, was qualified in this study conducted under IRB171883XX (approved on November 2017 by UCSD human Research Protection Program, under the title "Unused liver from deceased donors: role of myofibroblasts in liver fibrosis").[34] For hepatocytes isolation, the livers were placed on top of an ice pan covered by a plastic bag and then a sterile hood. Catheters were inserted into the major portal and/or hepatic vessels, and the tissue was perfused with cold organ-preservation solution or EMEM (Corning Cellgro cat no. 15-010-CM) + 25mM HEPES (Corning Cellgro cat. no. 25-060-CI). The catheters were then secured into the vessels either by sutures or surgical-grade glue. The liver tissue was then placed in a sterile plastic bag and connected to a peristaltic pump, and the tissue was perfused with HBSS (without calcium and magnesium or phenol red) (Hyclone cat no. SH30588.02) supplemented with 1.0mM EGTA without recirculation for 10–20min. Finally, the liver specimen was perfused with DMEM containing 0.1mg ml^{-1} of collagenase (VitaCyte cat no. 001-2030) and 0.02mg ml^{-1} of protease (VitaCyte cat. no. 003-1000). Perfusion was stopped when the liver tissue began to show fissures and separation from the liver capsule. The liver tissue was then removed from the plastic bag and placed in a sterile plastic beaker that contained warmed (37°C) DMEM supplemented with 5% FBS, 1% sodium pyruvate and 1% antibiotic. The cell suspension was filtered through sterile nylon-mesh-covered funnels to remove cellular debris and clumps of undigested tissue. Hepatocytes were isolated by low-speed centrifugation at 80g for 5min at 18°C. The hepatocyte pellets were gently resuspended in a Percoll (Sigma cat. no. GE17-0891-09) gradient and centrifuged at 100g for 10 minutes at 18°C. The supernatant was removed by aspiration, and the pellets were saved and resuspended in warmed (37°C) DMEM and the centrifugation step was repeated. The hepatocytes were plated in collagen coated 6-wells and after attached, were incubated with shCtrl and shFBP1 lentivirus for 24 h. After recovery for 24-48 h, the cells were stimulated with insulin for the indicated times and concentrations after 6 h of serum starvation.

METHOD DETAILS

Constructs

V5-FBP1, V5-FBP1^{E98A} and FBP1 truncation mutations (ΔE1-ΔE7) were generated in Dr. M. Celeste Simon's lab. Flag-ALDOB, Flag-PP2A-C, HA-AKT1 were kindly provided by Drs. Huiyong Yin (Chinese Academy of Sciences, Shanghai, China) and Alexandra C. Newton (University of California at San Diego, USA), respectively. FBP1 (TRCN0000050034, TRCN0000050035) and PP2A-C (TRCN0000002483, TRCN0000002486) shRNAs were purchased from Sigma. SgALDOB was constructed by cloning the guide sequences into the BsmBI site of the lentiCRISPR v2-puro vector. Human FBP1 mutants were constructed by Q5 Site-Directed Mutagenesis Kit (NEB, E0554S) in the PCDH-V5-FBP1 vectors. Primers are listed in Tables S1 and S2.

Plasmid transfection and virus infection

Expression vectors were transfected into 293T cells or HCC cell lines using Lipofectamine 3000 (Invitrogen, L300008) following the manufacturer's protocol. Lentiviruses were produced by co-transfecting PSPAX2 (4 μg), PMD2.G (4 μg) and PCDH-V5-FBP1 (8 μg) or FBP1 mutants (8 μg), PLKO.1 (8 μg) or lentiCRISPERv2 (8 μg) vectors. After 8 h medium was changed and fresh DMEM plus 10% FBS was added. Virus containing media were harvested 48-64 h later and filtered by 0.45 μm Steriflip filter (Millipore). HepG2 and Huh7 cells were infected with 1 ml virus containing medium with 8 μg/ml polybrene for 24 h. Cells were allowed to recover in complete medium for 24-48 h and then selected with puromycin. After 48 h surviving cell pools were used in the different experiments.

Immunoblot analysis and nuclear extraction

Cells were harvested and lysed in RIPA buffer (50 mM Tris-HCl, pH 7.4, 150 mM NaCl, 1% Triton X-100, 1% sodium deoxycholate, 0.1% SDS, 1 mM EDTA) supplemented with complete protease inhibitor cocktail.[35] Livers were homogenized in a Dounce homogenizer (Thomas Scientific, NJ) with 30 strokes in RIPA buffer with complete protease inhibitor cocktail. The proteins separated by SDS-PAGE and transferred to polyvinylidene difluoride (PVDF) membranes, blocked in 5% nonfat milk, and incubated with the indicated primary antibodies overnight. Second antibodies were added for another 1h and detected with Clarity Western ECL Substrate (Biorad). Immunoreactive bands were exposed in an automatic X-ray film processor. Nuclear extraction was performed with the NE-PER™ Nuclear and Cytoplasmic Extraction Reagent kit (Thermo Fisher, 78833), following manufacturer's instructions. After extraction, nuclear and cytoplasmic extracts were separated by SDS-PAGE and analyzed by immunoblotting as above.

Histology

Livers were dissected, fixed in 4% paraformaldehyde and embedded in paraffin. 5 μm thick sections were stained with hematoxylin and eosin (H&E) (Leica, 3801615, 3801571). For frozen block preparation, livers were embedded in Tissue-Tek OCT compound (Sakura Finetek), sectioned, and stained with Oil Red O to visualize TG accumulation. Liver PAS staining was performed with PAS kit (Thermo Fisher Scientific, #87007), using the manufacture's protocol.

Measurements of metabolites and hormones

Liver TG, serum TG and serum cholesterol were measured with Triglyceride Colorimetric Assay Kit (Cayman Chemical #10010303) and Cholesterol Fluorometric Assay Kit (Cayman Chemical #10007640), respectively, according to manufacturer protocols. Serum insulin and glucagon concentrations were determined by Mouse Insulin ELISA KIT (Invitrogen, EMMINS) and Glucagon Quantikine

ELISA Kit (R&D Systems, DGCG0), respectively, following manufacturer protocols. Liver NADPH and NADP were measured by NADP/NADPH-Glo™ Assays (Promega #G9081) according to manufacturer's protocol. ALT and AST assays were performed with ALT(GPT) Reagent (Thermo Scientific™, TR71121) and AST/GOT Reagent (Thermo Scientific™, TR70121), respectively, according to the manufacturer's protocol. ATP, Acetyl-CoA and G6P concentrations were determined by ATP assay kit (Abcam, ab83355), Acetyl-Coenzyme A Assay Kit (Sigma, MAK039) and PicoProbe™ Glucose-6-Phosphate Fluorometric Assay Kit (Biovision, K687), respectively according to the manufacturers protocols. Glucose and lactate were measured with Glucose colorimetric assay kit (Cayman Chemical #10009582) and Lactate Colorimetric/Fluorometric Assay Kit (Biovision, K607), respectively, according to the manufacturer's protocols.

[U-^{13}C] glucose, ^{13}C-lactate and D_2O labeling

D-glucose (U-^{13}C6, 99%) and ^{13}C-lactate were purchased from Cambridge Isotope Laboratories (NC9337143, CLM-1579). 8 wo *Fbp1*$^{F/F}$ and *Fbp1*$^{\Delta Hep}$ mice were fasted overnight from 6 pm-10 am and 45 min before sacking were injected intravenously (i.v.) with 500 mg/kg [U-^{13}C] glucose.as previously described.[36,37] For lactate labeling, mice were i.v. injected with 0.5mg/g sodium L-lactate (^{13}C3) for 3 times 1h before sacking.[38] Liver and serum were collected for metabolomic analysis. To measure DNL, 8 wo *Fbp1*$^{F/F}$ and *Fbp1*$^{\Delta Hep}$ mice were i.p. injected with 0.035 ml/body weight D_2O (Sigma) in 0.9% NaCl, and drinking water was replaced with 8% enriched D_2O.[39] Mice were given D_2O for 22-24h and starved for 16 h before sacrifice, plasma and liver were collected and immediately snap-frozen in liquid nitrogen.

Stable-Isotope Tracer Metabolomics

Sample extraction methods: Frozen liver samples of *Fbp1*$^{F/F}$ and *Fbp1*$^{\Delta Hep}$ (~40 mg) were transferred to 2-mL tubes containing 2.8 mm ceramic beads (Omni International) and 0.45 ml ice-cold 50% methanol/ 20 μM L-norvaline was added. Tubes were shaken (setting 5.5) for 30 s on a Bead Ruptor 12 (Omni International), quickly placed on ice, and frozen at -80°C overnight. Thawed samples were centrifuged at 15,000 x g for 10 minutes at 4°C. The supernatant was then transferred to a new tube, mixed with 0.225 ml chloroform, and centrifuged at 10,000 x g for 10 minutes at 4°C. This produced a two-phase separation. Portions (100 μl) of the top phase were dried (Speedvac) for analyses of polar metabolites. The lower phase was dried (Speedvac) for analysis of fatty acids. Plasma samples (5 or 10 μl) were mixed with 4 volumes of acetone (pre-cooled to -20°C), left at -20°C for 1 h, and centrifuged at 14,000 x g for 10 minutes at 4°C. Supernatants were dried by Speedvac.

Metabolite derivatization and GC-MS run conditions: Polar metabolites except for glucose and sugar-phosphates were derivatized using isobutylhydroxylamine and MTBSTFA, and analyzed by GC-MS as described.[40] Plasma samples for glucose analysis were derivatized first with 30 μl ethylhydroxylamine (Sigma) at 20 mg/ml in pyridine for 20 min at 80°C, and secondarily with 30 μl BSTFA (Thermo) for 60 min at 80°C. Samples were transferred to autosampler vials with inserts and analyzed using an Rxi-5ms column (15 m x 0.25 i.d. x 0.25 μm, Restek) installed in a Shimadzu QP-2010 Plus gas chromatograph-mass spectrometer (GC-MS). The GC-MS was programmed with an injection temperature of 250°C, 1.0 μl injection volume and split ratio 1/10. The GC oven temperature was initially 130°C for 4 min, rising to 230°C at 6°C/min, and to 280°C at 60°C/min with a final hold at this temperature for 2 min. GC flow rate, with helium as the carrier gas, was 50 cm/s. The GC-MS interface temperature was 300°C and (electron impact) ion source temperature was 200°C, with 70 eV ionization voltage. The main glucose peak eluted at 13.7 min, and fragments of m/z 319 (contains 4 glucose carbons; $C_{13}H_{31}O_3Si_3$) and m/z 205 (contains 2 glucose carbons; overall formula $C_8H_{21}O_2Si_2$) were used to analyze ^{13}C-glucose labeling as described.[40] Liver samples labeled with ^{13}C-lactate for sugar-phosphate analysis were derivatized first with 30 μl pentafluorobenzyl-hydroxylamine (Alfa Aesar) 20 mg/ml in pyridine for 60 min at 37°C, and secondarily with 30 μl BSTFA (Thermo) for 60 min at 37°C. The GC-MS method was as described above, except that injection volume was 2 μl, and initial GC oven temperature was 200°C for 4 min, rising to 280°C at 8°C/min, with a final hold at this temperature for 2 min. F6-P eluted as a pair of peaks at 10.33 and 10.49 min. The earlier peak was analyzed for ^{13}C-labeling (fragment of m/z 459 containing 3 glucose carbons; $C_{15}H_{40}O_6Si_4P$). Fatty acids (palmitate and stearate) were derivatized and analyzed for labeling as described (the methyl stearate ion m/z 298 was analyzed).[40]

Size Exclusion Chromatography

Liver samples were fractionated on a Superdex 200 HR 10/30 column (Pharmacia Biotech, Cat # 17-1088-01) using an AKTA FPLC system (GE). Column was equilibrated with and samples were fractionated in CHAPS lysis buffer (25mM HEPES pH 7.4, 150mM NaCl, 1mM EDTA, and 0.3% CHAPS). 0.5 mL of sample at 10 mg/mL (5mg protein total) in CHAPS lysis buffer was injected onto the column and fractionated at a 0.5 mL/min flow rate over 1.2 column volumes. 0.25 mL fractions were collected. The injection loop was thoroughly rinsed, and blank runs were performed between each sample.

Molecular weights ranges within fractions were approximated through comparison with a standard curve (Kav of protein standards v. log(MW)). Kav of Gel Filtration Protein Standards (Bio-Rad, Cat#1511901) of known molecular weight were determined under identical fractionation conditions as described for samples and calculated using the following equation where Ve is elution volume, Vo is void volume, and Vt is the total volume of the column:

$$K_{av} = \frac{Ve - Vo}{Vt - Vo}$$

Please cite this article in press as: Gu et al., Fructose-1,6-bisphosphatase is a nonenzymatic safety valve that curtails AKT activation to prevent insulin hyperresponsiveness, Cell Metabolism (2023), https://doi.org/10.1016/j.cmet.2023.03.021

Elution volumes were determined by monitoring inline absorbance at 280 nm as the standards eluted. Peak elution volumes were determined using Unicorn 5.1 Software (GE). Void volume was similarly determined by monitoring elution of 1 mg of blue dextran (Sigma D4772). Total volume of the column was provided by the manufacturer.

FBP1 activity assay

FBP1 activity was measured with Fructose-1,6-Bisphosphatase Activity Assay Kit (Colorimetric) (Abcam, ab273329). Briefly, 20 μg lysates of control Huh7 cells, or Huh7 cells expressing WT and mutant forms of FBP1 were prepared in 500 μl ice-cold FBP assay buffer. $(NH_4)_2SO_4$ was used to precipitate the proteins and remove small molecules that could interfere with the assay. The precipitated proteins were spun down and resuspend in FBP assay buffer. The samples were incubated with the reaction mix containing FBP converter, FBP probe, FBP developer and FBP substrate and absorbance at OD=450 was measured in a kinetic mode for 5-60 min at 37°C. FBP1 activity was normalized according to its expression level determined by immunoblotting.

GTT, PTT, and ITT

For GTT and PTT, *Fbp1*$^{F/F}$ and *Fbp1*$^{\Delta Hep}$ mice that were HFD fed for 12 wk or NCD-8 wo mice were fasted for 12-14 h and then given 1 g/kg glucose or sodium pyruvate (2 g/kg, Sigma) by i.p. injection. Blood glucose was measured before injection and every 30 min thereafter with a glucometer (OneTouch Ultra 2, One Touch) on blood from superficial tail incision. 8 wo *Fbp1*$^{F/F}$ and *Fbp1*$^{\Delta Hep}$ mice or 18 wo *Fbp1*$^{F/F}$ and *Fbp1*$^{\Delta Hep}$ mice that were HFD fed for 12 wk, fasted for 2-4 h then injected with 0.5 U/kg insulin. Blood glucose was measured before injection and every 30 min thereafter, up to 2 h.

Glycogen extraction

Small pieces of livers were weighted at dissection. Samples were boiled for 30 min in 500 μl of 30% KOH solution with Vortex every 10 min. 100 μl of 1 M Na_2SO_4 were added when the samples were cooled down. 1.2 ml of 100% ethanol was added, and the samples cooked for 5 min at 95°C. The samples were then centrifuged for 5 min at 16,000xg. Pellets were washed twice by resuspension in 500 μl of double-distilled water, 1 ml 100% ethanol, and centrifugation. Following the last wash, pellets were air-dried and resuspended in 100 μl of 50 mM sodium acetate at pH 4.8 containing 0.3 mg/ml amyloglucosidase. The samples were incubated at 37°C overnight on a shaker to facilitate digestion. Fujifilm Autokit glucose assay (997-03001) was used to determine the amount of glycogen by comparing it to a standard curve. The content of glycogen was normalized to tissue weight.

Glycogen Synthase Activity

Freeze-dried liver tissue (20g-30mg) was homogenized in ice-cold buffer (50 mM Tris-HCl (pH 7.8), 100 mM NaF, 10 mM EDTA). Homogenates were centrifuged for 5 min at 3600g at 4°C and GYS activity measured in supernatants with 0 or 12 mM of added G6-P.[41] Next, the Transcreener®UDP^2 FI Assay Kit (BellBrook, 3019-A) was used to measure GYS activity by measuring the release of UDP from UDP-glucose.

Measuring liver protein synthesis with O-propargyl-puromycin

8-wo *Fbp1*$^{F/F}$ and *Fbp1*$^{\Delta Hep}$ mice were starved for 4-6 h starting at 6 pm and then i.p. injected with 100 μl of a 20 mM solution of O-propargyl-puromycin (OP-Puro, MedChemExpress, HY-15680) in PBS.[42] Livers were harvested after 1 h, fixed in formalin and paraffin embedded samples were cut into 5 μm sections. OPP incorporation was detected by staining with Click-&-Go Plus 488 OPP Protein Synthesis Assay Kit (Click Chemistry, #1493), following manufacturer's instructions. Briefly, liver sections were deparaffinized with xylene, hydrated with ethanol and incubated with a reaction cocktail containing copper catalyst, AZDye Azide plus solution and reducing agent for 20 min, while protected from light. DNA was stained with Hoechst 33342 and the sections imaged on a confocal microscope. The intensity of fluorescent-labeled protein-incorporated OPP was quantified by automated analysis of microscopic images with Image J software (NIH).

Generation and infection by AAV8-FBP1, AAV8-FBP1^{E98A} and AAV8-Ctrl virus

pAAV[Exp]-CAG>mFbp1WT:T2A:EGFP:WPRE and pAAV[Exp]CAG>HA/mFbp1^{E98A}:T2A: EGFP:WPRE were constructed by Vectorbuilder. AAV8-mFBP1, AAV8-mFBP1^{E98A} and AAV8-Ctrl viruses were generated by Vectorbuilder. Briefly, 293T cells were co-transfected with indicated vectors and Rep-cap plasmid and helper plasmids. After 50-60 h, cell lysates were harvested and concentrated by PEG precipitation and CsCl gradient ultracentrifugation. 6-8 wo mice were infected with AAV8-mFBP1, mFBP1^{E98A} and AAV8-Ctrl (10^{12} virus copies per mouse) via tail vein injection. Liver and serum were collected 3 weeks later.

Primary mouse hepatocytes isolation

8-wo male *Fbp1*$^{F/F}$ and *Fbp1*$^{\Delta Hep}$ mice were fasted for 14-16 h and primary hepatocytes were isolated using a two-step collagenase perfusion as described.[43] Briefly, mice livers were perfused with perfusion buffer (HBSS (Thermo Fisher, 14175095) with 0.5mM EDTA and 25mM HEPES) and digested with digestion buffer (HBSS with Ca^{2+} Mg^{2+} (Thermo Fisher, 24020117), 25mM HEPES and 1mg/ml Liberase). The hepatocytes were spun down at 50g for 3 min at 4 °C then purified on a Percoll gradient. The hepatocytes

Please cite this article in press as: Gu et al., Fructose-1,6-bisphosphatase is a nonenzymatic safety valve that curtails AKT activation to prevent insulin hyperresponsiveness, Cell Metabolism (2023), https://doi.org/10.1016/j.cmet.2023.03.021

were counted and directly collected or plated on collagen-coated plates for 6 h in plating medium (DMEM low glucose, 5%FBS and 1% Penicillin-streptomycin (PS)). After cell attachment, the plating medium was replaced with maintenance medium (Willams E medium, 2 mM glutamine and 1% PS) for further use.

Proximity ligation assays (PLA)

FBP1:ALDOB:PP2A-C:AKT interactions in liver tissue were detected with an *in situ* PLA kit (Duolink® In Situ Red Starter Kit Mouse/Rabbit, Sigma, DUO92101).[44] Briefly, paraffin embedded tissue sections were deparaffinized with 3x washes with xylene, rehydrated with ethanol and subjected to antigen unmasking with citrate buffer at 95-98 °C for 15 min. Tissues were incubated with 3% H_2O_2 for 10 min and then blocked with Duolink blocking solution at 37 °C for 60 min. The samples were incubated with primary antibodies overnight, and then incubated with the PLA Probe, ligase and polymerase following manufacturer's instructions. Tissues were mounted with an *in situ* mounting medium with DAPI and images captured on a TCS SPE Leica confocal microscope. The results were quantified by counting dots per field in 3 randomly selected fields of view.

Immunoprecipitation and mass spectrometry analysis

For immunoprecipitation (IP) experiments, cells and livers were harvested in lysis buffer (20 mM Tris-HCl, pH 7.5, 1% NP-40, 137 mM NaCl, 1 mM $MgCl_2$, 1 mM $CaCl_2$, 10% glycerol) supplemented with complete protease inhibitor cocktail. Cell and liver lysates were pre-cleared with 30 μl protein G beads (Life Technologies), and then incubated with 2 μg isotype matched IgG control or indicated antibodies on a rocking platform overnight at 4°C. 50 μl protein G were added and incubated for another 2-3 h. The immunocomplexes were washed 5x with lysis buffer, separated by SDS-PAGE and analyzed by immunoblotting as above.

For mass spectrometry analysis, *Fbp1*$^{\Delta Hep}$ mouse livers transduced with AAV-FBP1 or AAV-Control were homogenized in NP-40 lysis buffer. Lysates were IP'ed with HA antibody using magnetic beads. The IP's were washed twice with 1xPBS (Gibco) and resuspended in 150 uL 5% formic acid to denature proteins and remove them from the beads. The supernatants were placed in new tubes and 1.5 mL HPLC-grade water was added and then dried down in a concentrator (Thermo SpeedVac). Dried samples were resuspended in 250 uL 1M urea, reduced with 5 uL of 500 mM dithiothreitol (DTT) and placed on a 47°C block for 30 minutes. Samples were then cooled to room temperature and 15 μL 500 mM iodoacetamide to alkylate proteins were added and the samples were kept in the dark for 45 minutes. The reactions were quenched with 5 uL 500 mM DTT. 1M Tris-HCl was added to adjust the pH and 5 μL trypsin (2.5 ug, Promega Sequence Grade) was added and the samples digested overnight at 37°C. 80 μL of 1% TFA was added to stop the digestion and the samples were dried down. The samples were then resuspended in 100 μL 0.1% formic acid (FA) desalted using C18 discs in a pipette tip ("Stage Tips"). The eluted peptides were then quantified (Thermo PepQuant) and 9 μg of peptides were transferred to a new tube and dried down. These samples were then resuspended in 9 μL 5% acetonitrile and 5% FA and were placed in MS inserts for proteomic characterization. Sample spectra were collected on a Thermo Fusion mass spectrometer that collected MS data in positive ion mode within the 400 to 1,500 m/z range. Mass spectra raw files were first searched using Proteome Discoverer 2.2 using the built-in SEQUEST search algorithm. Built-in TMT batch correction was enabled for all samples.

In vitro binding assay

In vitro binding assay was performed as described previously.[23] In brief, recombinant GST-PP2A-C protein were incubated with His-AKT, His-ALDOB and His-FBP1 in binding buffer (25mM Tris-HCl, 200 Mm NaCl, 1mM EDTA, 0.5% NP-40, 10μg/μl BSA and 1mM DTT). GST, AKT or FBP1 antibodies and protein A/G beads were mixed and incubated overnight. The lysates were washed with ice-cold binding buffer for 3 times and boiled before subjected to IB analysis.

PP2A dephosphorylation assay

The PP2A dephosphorylation assay were performed as described.[23] Briefly, Huh7 cells stably expressing HA-AKT1 or HA-c-Myc were serum starved for 6 h and stimulated with insulin (100nM) or EGF (100ng/ml) for 1 h, respectively. Cells were harvested and AKT1 or c-Myc was IP'ed with an HA antibody. The immunoprecipitates were washed and resuspended in PP2A phosphatase assay buffer (20mM HEPES, 100mM NaCl and 3mM DTT). Together with recombinant ALDOB, FBP1 or FBP1^{E98A} and active PP2A, the AKT1 or c-Myc IPs were incubated at 30°C for the indicated times and AKT1 and c-Myc phosphorylation was assessed by IB analysis.

Peptide synthesis and treatment

Cell permeable Scrambled (Ctrl) and FBP1 peptides were synthesized by Biomatik. Male BL6 mice were HFD fed for 14 weeks from week 7 postnatally. Mice were i.p. injected with the Ctrl and FBP1 peptides (10mg/kg each) every 2 days for 2 weeks. Mice were fasted overnight before being subjected to GTT and PTT and fasted 2h before ITT.

Protein structure predictions and peptide docking

AKT1, PP2A-C, ALDOB, FBP1 and FBP1 E7 peptide structure modeling were performed with the ColabFold implantation of AlphaFold (https://alphafold.ebi.ac.uk/).[45] The best positions for peptide and protein interactions were explored, and hydrogen bonds and amino acids were identified and labeled in PyMOL (https://pymol.org/2/).

RNA isolation and quantitative real-time PCR (Q-PCR)

Total liver RNA was extracted with RNeasy Plus Mini kit (Qiagen #74134) and cDNA was synthesized with SuperScript™ VILO™ cDNA Synthesis Kit (Thermo Fisher Scientific, 11754050).[43] mRNA expression was determined by CFX96 thermal cycler (Biorad). Data are presented as arbitrary units and calculated by comparative CT method ($2Ct^{(18s\ rRNA-gene\ of\ interest)}$). Primers are listed in Table S3.

QUANTIFICATION AND STATISTICAL ANALYSIS

Data are presented as mean ± SD or mean ± SEM as indicated. Differences between mean values were analyzed by unpaired two-tailed Student's t test with GraphPad Prism software. P value<0.05 was considered as significant (*$p < 0.05$, **$p < 0.01$, ***$p < 0.001$, ****$p < 0.0001$, n.s., $p \geq 0.05$).

Cell Metabolism, Volume *35*

Supplemental information

Fructose-1,6-bisphosphatase is a nonenzymatic safety valve that curtails AKT activation to prevent insulin hyperresponsiveness

Li Gu, Yahui Zhu, Kosuke Watari, Maiya Lee, Junlai Liu, Sofia Perez, Melinda Thai, Joshua E. Mayfield, Bichen Zhang, Karina Cunha e Rocha, Fuming Li, Laura C. Kim, Alexander C. Jones, Igor H. Wierzbicki, Xiao Liu, Alexandra C. Newton, Tatiana Kisseleva, Jun Hee Lee, Wei Ying, David J. Gonzalez, Alan R. Saltiel, M. Celeste Simon, and Michael Karin

Supplementary Materials for

Fructose-1,6-bisphosphatase is a nonenzymatic safety valve that curtails AKT activation to prevent insulin hyperresponsiveness

Li Gu *et al.*

Corresponding author: Michael Karin, karinoffice@ucsd.edu

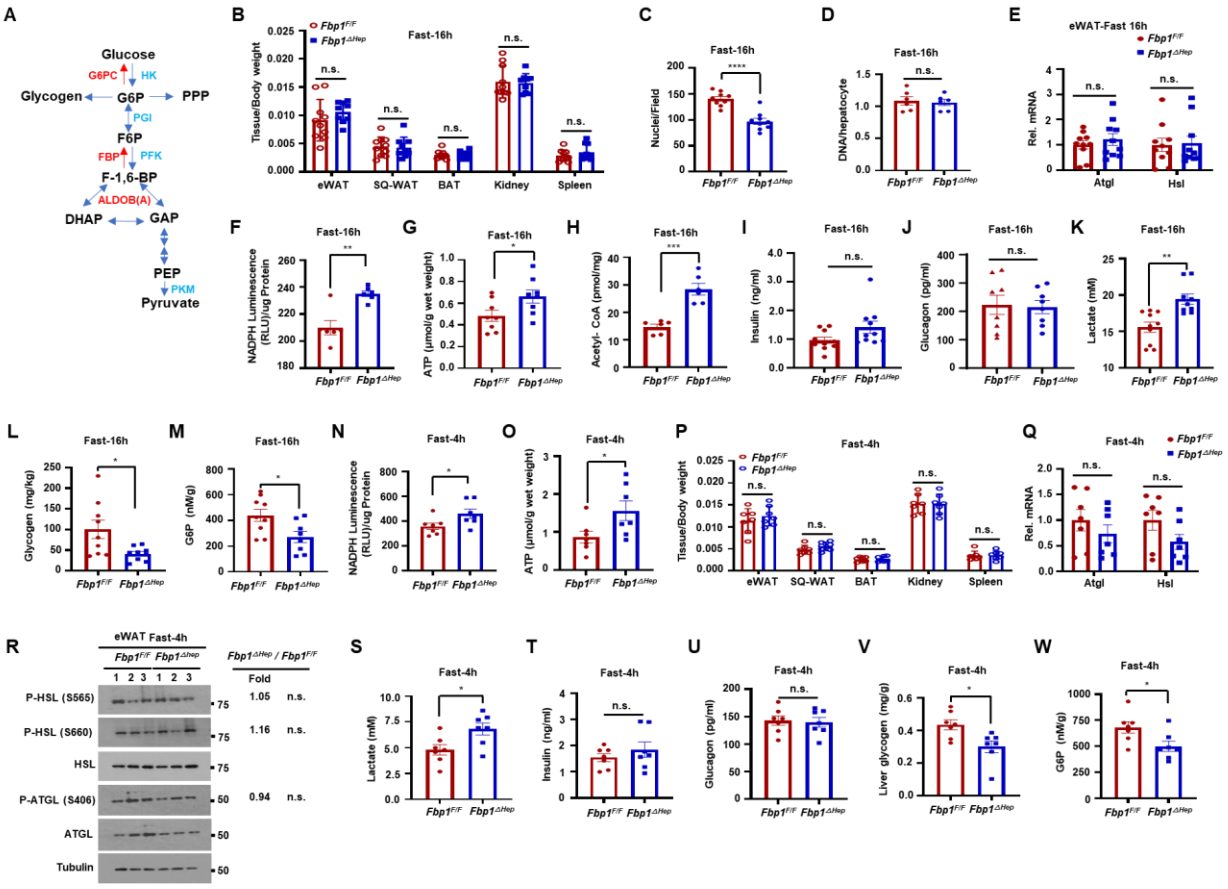

Figure S1. Hepatocyte specific FBP1 ablation increases ATP, acetyl-CoA and serum lactate while decreasing glycogen and G6-P amounts after 16h and 4h fast, Related to Figure 1.

(A) Schematic representation of glucose metabolism and roles of FBP1 and ALDOB in GNG.

(B) Epididymal white adipose tissue (eWAT), subcutaneous adipose tissue (SQ-WAT), brown adipose tissue (BAT), kidney and spleen weight/body weight ratio in 16 h fasted 8-wo *Fbp1*$^{F/F}$ and *Fbp1*$^{\Delta Hep}$ mice (n=9-10).

(C and D) Nuclei per field (C) and hepatocyte DNA content (D) from 16 h fasted 8-wo *Fbp1*$^{F/F}$ and *Fbp1*$^{\Delta Hep}$ livers (n=6-9).

(E) qRT-PCR analysis of lipolytic mRNAs in eWAT of 16 h fasted 8-wo *Fbp1*$^{F/F}$ and *Fbp1*$^{\Delta Hep}$ mice (n=9-10).

(F-H) NADPH (F), ATP (G) and acetyl-CoA (H) concentrations of liver lysates from above mice (n=6-8).

(I and J) Serum insulin (I) and glucagon (J) in indicated mice (n=6-8).

(K-M) Serum lactate (K), liver glycogen (L) and G6-P (M) in indicated mice (n=9-10).

(N and O) NADPH (N) and ATP (O) concentrations in liver lysates of 4 h fasted 8-wo *Fbp1*$^{F/F}$ and *Fbp1*$^{\Delta Hep}$ mice (n=7).

(P) eWAT, SQ-WAT, BAT, kidney, and spleen weight/body weight ratio in 4 h fasted 8-wo *Fbp1*$^{F/F}$ and *Fbp1*$^{\Delta Hep}$ mice (n=7).

(Q) qRT-PCR of lipolytic mRNAs in eWAT of 4 h fasted 8-wo *Fbp1*$^{F/F}$ and *Fbp1*$^{\Delta Hep}$ mice (n=7).

(R) IB analysis of indicated proteins in eWAT of 4 h fasted 8-wo *Fbp1*$^{F/F}$ and *Fbp1*$^{\Delta Hep}$ mice. Densitometry determined relative normalized protein ratios (*Fbp1*$^{\Delta Hep}$/*Fbp1*$^{F/F}$) and P values are shown on the right.

(S-U) Serum lactate (S), insulin (T) and glucagon (U) in the indicated mice (n=7).

(V and W) Liver glycogen (V) and G6-P (W) in the indicated mice (n=7).

Data are presented as mean ± SEM. *P < 0.05, **P < 0.01, ***P < 0.001, ****p < 0.0001 (Unpaired two-tailed t test). n.s., not significant.

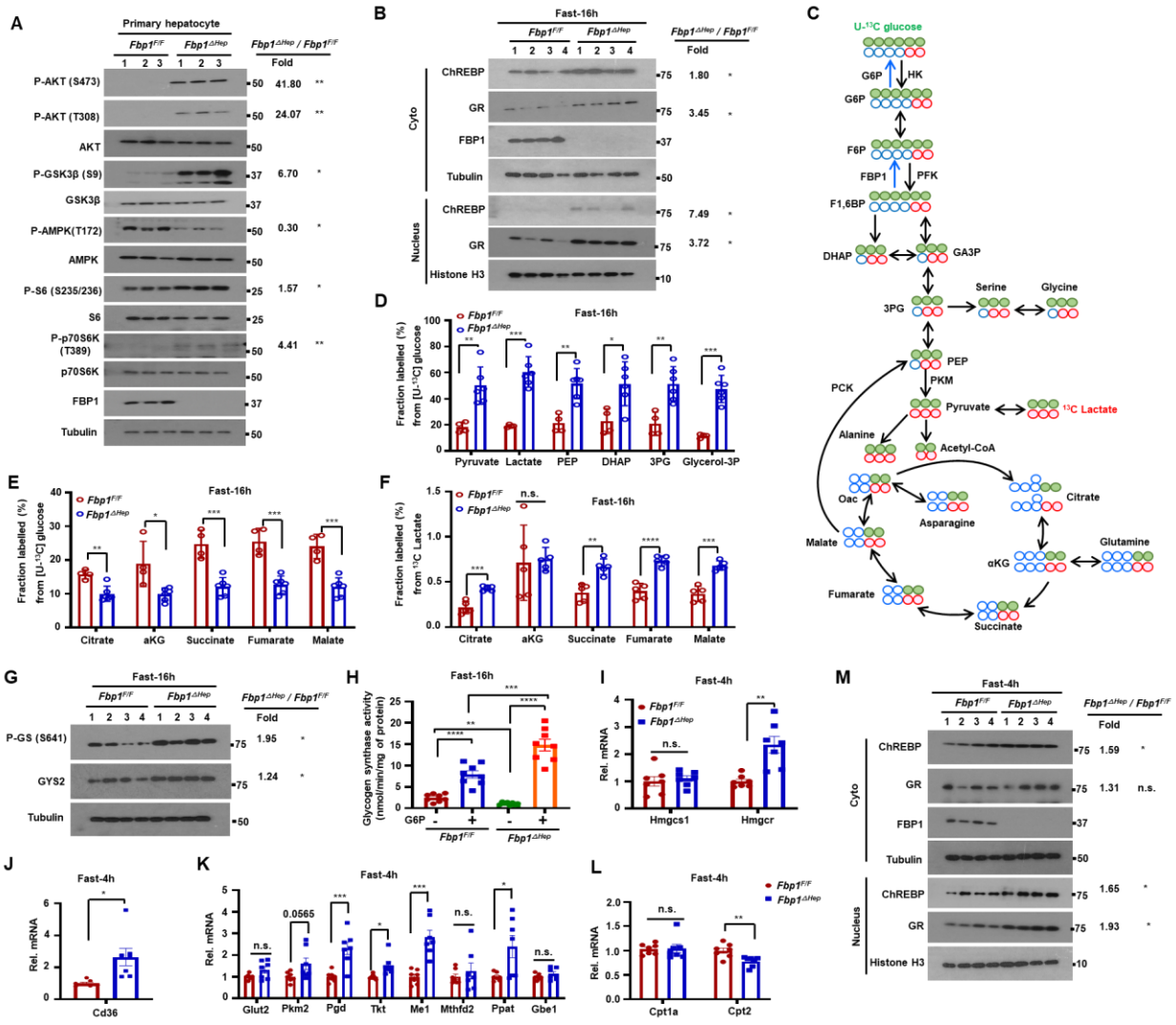

Figure S2. Fasting induced metabolic genes and metabolic alterations in *Fbp1*$^{\Delta Hep}$ mice, Related to Figure 2.

(A) IB analysis of mouse primary hepatocytes from fasted 8-wo *Fbp1*$^{F/F}$ and *Fbp1*$^{\Delta Hep}$ mice. Relative normalized protein ratios (*Fbp1*$^{\Delta Hep}$/*Fbp1*$^{F/F}$) and P values are shown on the right.

(B) IB analysis of nuclear and cytosolic liver proteins in 16 h fasted 8-wo *Fbp1*$^{F/F}$ and *Fbp1*$^{\Delta Hep}$ mice. Relative normalized protein ratios (*Fbp1*$^{\Delta Hep}$/*Fbp1*$^{F/F}$) and P values are shown on the right.

(C) Schematic of U-^{13}C glucose and ^{13}C-Lactate tracing of 16 h fasted 8-wo *Fbp1*$^{F/F}$ and *Fbp1*$^{\Delta Hep}$ livers (n=4-6).

(D and E) Fractional labelling of glycolytic (D) and TCA (E) metabolites from U-^{13}C glucose tracing of fasted 8-wo *Fbp1*$^{F/F}$ and *Fbp1*$^{\Delta Hep}$ liver (n=4-6).

(F) Fractional labelling of liver TCA intermediates from ^{13}C-lactate tracing of indicated livers (n=5).

(G) P-GS(S641) and GYS2 in liver lysates of fasted 8-wo *Fbp1*$^{F/F}$ and *Fbp1*$^{\Delta Hep}$ mice. Relative normalized relative GYS2 and P-GYS2 ratios (*Fbp1*$^{\Delta Hep}$/*Fbp1*$^{F/F}$) and P values are shown on the right.

(H) Glycogen synthase activity in lysates of 16 h fasted 8-wo *Fbp1*$^{F/F}$ and *Fbp1*$^{\Delta Hep}$ livers (-/+) saturating exogenous G6-P (n=7-8).

(I-L) qRT-PCR of cholesterol synthesis (I), lipid uptake (J), glycolysis, pentose phosphate pathway, glycogen synthesis (K) and β-oxidation (L) related mRNAs in livers of 4 h fasted 8-wo *Fbp1*$^{F/F}$ and *Fbp1*$^{\Delta Hep}$ mice (n=7).

(M) IB analysis of nuclear and cytosolic extracts of 4 h fasted 8-wo *Fbp1*$^{F/F}$ and *Fbp1*$^{\Delta Hep}$ livers. Relative normalized protein ratios (*Fbp1*$^{\Delta Hep}$/*Fbp1*$^{F/F}$) and P values are shown on the right.

Data are presented as mean ± SEM, *P < 0.05, **P < 0.01, ***P < 0.001, ****p < 0.0001, n.s., not significant. (Unpaired two-tailed t test).

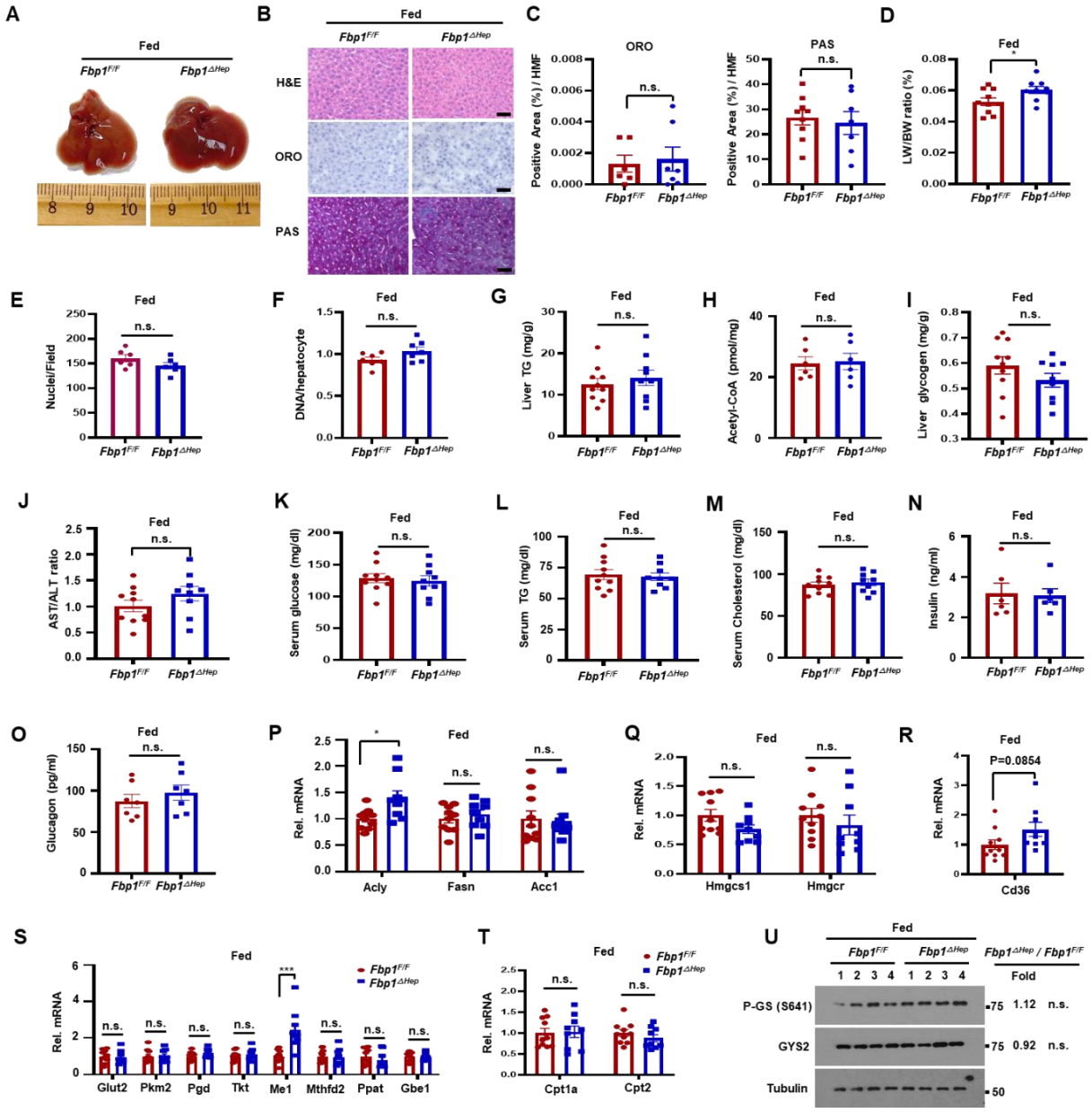

Figure S3. The fed *Fbp1*$^{\Delta Hep}$ liver is metabolically normal, Related to Figure 2.

(A) Gross morphology of livers from 8-weeks-old (wo) *Fbp1*$^{F/F}$ and *Fbp1* $^{\Delta Hep}$ mice at the fed (*ad libitum*) state (n=9-10).

(B) H&E, ORO, and PAS staining of liver sections from the mice in S3A. Scale bars, 20 μm.

(C) ORO and PAS staining intensity per HMF were determined by Image J analysis of the liver sections in S3B.

(D-M) Liver/body weight (D), nuclei per field (E), hepatocyte DNA content (F), and liver TG (G), acetyl-CoA (H) and glycogen (I), and serum AST/ALT ratio (J), glucose (K), TG (L), and cholesterol (M) in the indicated mice (n=6-10).

(N and O) Serum insulin (N) and glucagon (O) in the indicated mice (n=6-10).

(P-T) qRT-PCR of lipogenesis (P), cholesterol synthesis (Q), lipid uptake (R), glycolysis, pentose phosphate pathway, glycogen synthesis (S) and β-oxidation (T) related mRNAs in livers of fed 8-wo *Fbp1*$^{F/F}$ and *Fbp1*$^{\Delta Hep}$ mice (n=9-10).

(U) P-GS(S641) and GYS2 in liver lysates of fed 8-wo *Fbp1*$^{F/F}$ and *Fbp1*$^{\Delta Hep}$ mice. Relative normalized protein ratios (*Fbp1*$^{\Delta Hep}$/*Fbp1*$^{F/F}$) and P values are shown on the right.

Data are presented as mean ± SEM, *P < 0.05, ***P < 0.001, n.s., not significant. (Unpaired two-tailed t test).

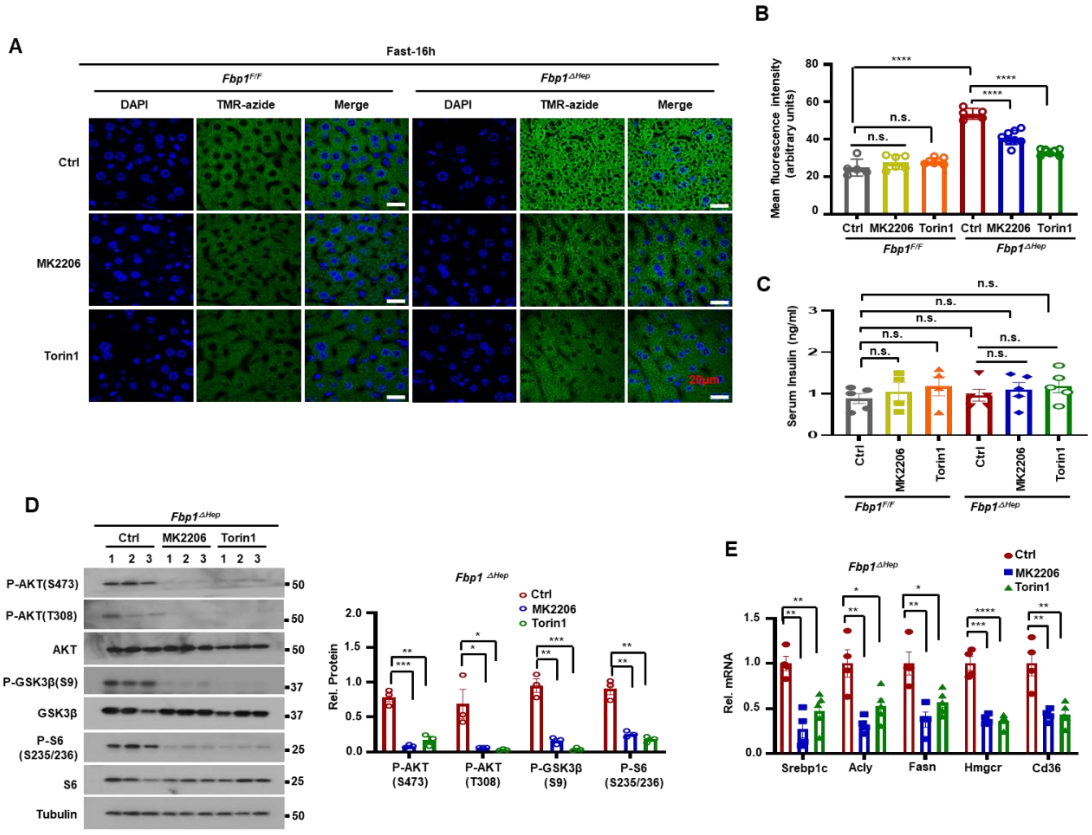

Figure S4. AKT and mTORC inhibitors attenuate hepatomegaly, hepatosteatosis and hyperlipidemia in fasted *Fbp1*$^{\Delta Hep}$ mice, Related to Figure 3.

(A-B) Liver protein synthesis in untreated or MK2206 or Torin1 pretreated and 16 h fasted 8-wo *Fbp1*$^{F/F}$ and *Fbp1*$^{\Delta Hep}$ mice was determined by OP-puro (TMR-azide) incorporation (A) (n=4-5). Scale bars, 20 μm. Mean fluorescence intensity of above liver sections (B).

(C) Serum insulin levels in the mice from Figure 3A (n=4-5).

(D) IB analysis of liver lysates from above mice (left) and relative normalized protein amounts (right).

(E) qRT-PCR of liver *Srebp1c*, *Acly*, *Fasn*, *Hmgcr* and *Cd36* mRNAs in the mice from Figure 3A (n=4-5).

Data are presented as mean ± SEM. *P < 0.05, **P < 0.01, ***P < 0.001, ****p < 0.0001, n.s., not significant. (Unpaired two-tailed t test).

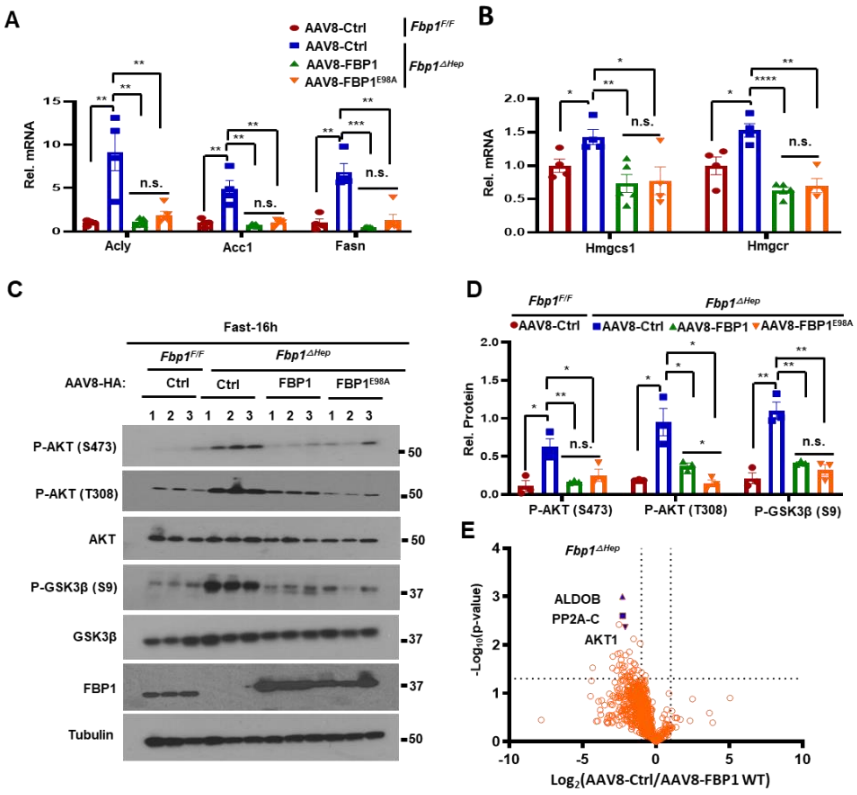

Figure S5. Catalytically inactive FBP1 restrains hepatomegaly, fatty liver, and hyperlipidemia, but not hypoglycemia in *Fbp1*$^{\Delta Hep}$ mice, Related to Figure 4.

(A and B) qRT-PCR of liver *Acly*, *Acc1*, *Fasn* (A), *Hmgcs1* and *Hmgcr* (B) mRNAs of fasted *Fbp1*$^{F/F}$ and *Fbp1*$^{\Delta Hep}$ mice transduced with AAV8-Ctrl, AAV8-FBP1 and AAV8-FBP1^{E98A} (n=4-5).

(C and D) IB analysis of liver lysates from the mice in Figure 4A (C) and relative normalized protein amounts (D).

(E) Scatterplots of FBP1 interacting proteins identified by MS analysis of HA IPs from *Fbp1*$^{\Delta Hep}$ livers transduced with AAV8-HA-control or AAV8-HA-FBP1. The liver lysates were immuno-purified on anti-HA affinity beads. The eluates were washed and analyzed by mass spectrometry. Data are presented as mean ± SEM. *P < 0.05, **P < 0.01, ***P < 0.001, ****p < 0.0001, n.s., not significant. (Unpaired two-tailed t test).

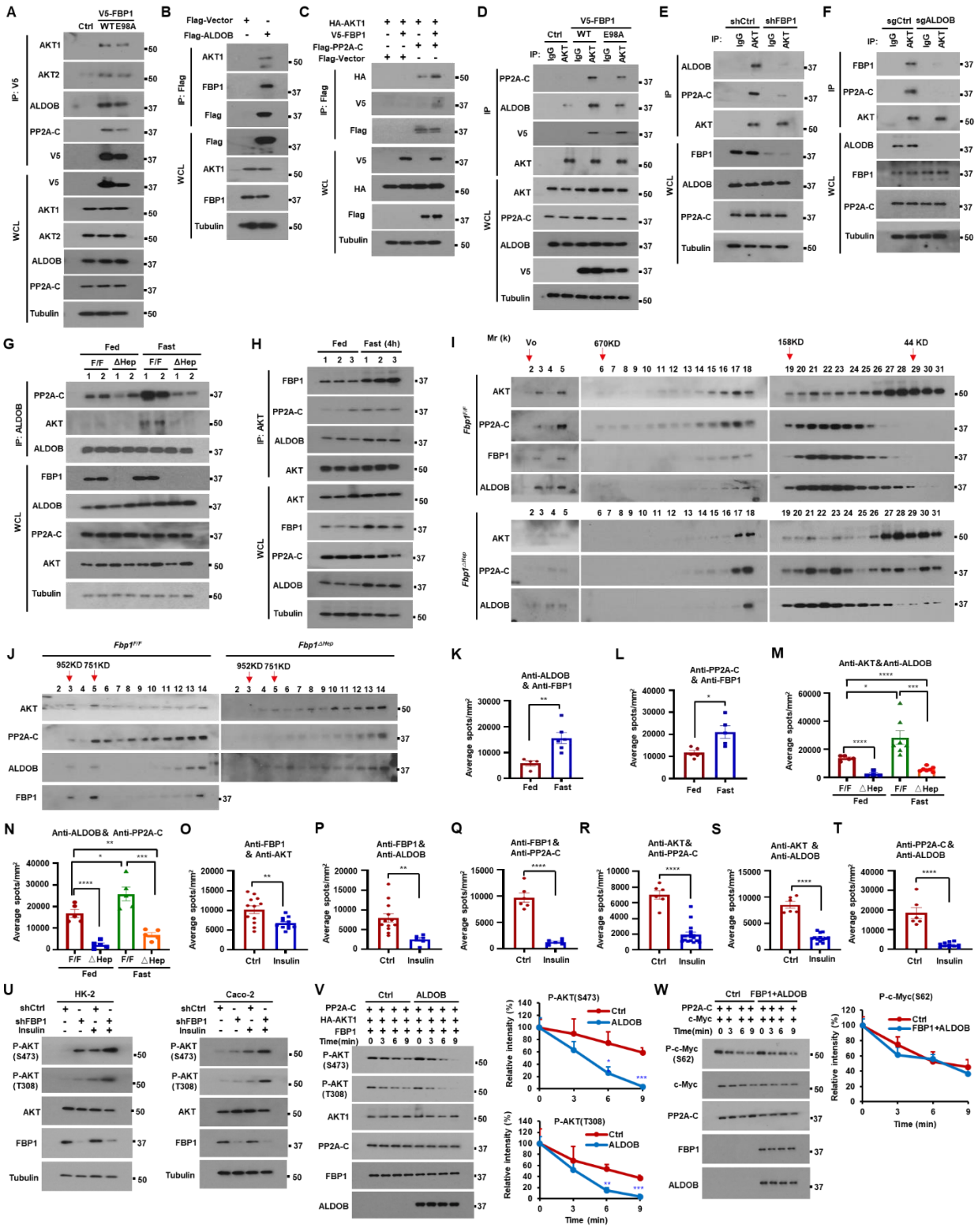

Figure S6. FBP1 associates with ALDOB and PP2A-C to form a protein complex that binds AKT and inhibits its activation, Related to Figure 5.

(A) IP analysis of 293T cells transfected with Ctrl, V5-FBP1 or V5-FBP1^{E98A} vectors. The gel separated IPs were IB'ed with the indicated antibodies.

(B) IP analysis of 293T cells transfected with empty Flag or Flag-ALDOB vectors. The gel separated IPs were IB'ed with the indicated antibodies.

(C) IP analysis of 293T cells transfected with HA-AKT1, V5-FBP1 and Flag-PP2A-C. The gel separated IPs were IB'ed with the indicated antibodies.

(D) IP analysis of Huh7 cells stably transfected with FBP1, FBP1^{E98A} or Ctrl vectors. The gel separated IPs were IB'ed with the indicated antibodies.

(E and F) IP analysis with indicated antibodies of Huh7 cells stably transfected with shCtrl, shFBP1 (E) and sgCtrl or sgALDOB (F). The gel separated IPs were IB'ed with the indicated antibodies.

(G and H) IP analysis of liver lysates from 8-wo *Fbp1*$^{F/F}$ and *Fbp1*$^{\Delta Hep}$ mice fed or fasted for 16 h (G) or 4h (H). The gel separated IPs were IB'ed with the indicated antibodies.

(I and J) Liver lysates of fasted 8-wo *Fbp1*$^{F/F}$ and *Fbp1*$^{\Delta Hep}$ mice were analyzed by gel filtration chromatography. Fractions were resolved by SDS-PAGE and probed with the indicated antibodies (I). Fractions 2-14 were analyzed again as above (J). Arrows indicate the approximate elution volumes of molecular weight standards: blue dextran, Vo; thyroglobulin, 670kDa; γ-globulin, 158kDa; ovalbumin, 44kDa; and myoglobin, 17kDa.

(K and L) Quantification of representative PLA images (n=5-12) of ALDOB-FBP1 (K) and PP2A-C-FBP1 (L) interactions determined with liver sections of fed or fasted (16 h) 8-wo WT mice stained with the indicated antibody combinations.

(M and N) Quantification of representative images of ALDOB-AKT (M) and ALDOB-PP2A-C (N) interactions detected by PLA of liver sections of fed or 16 h fasted 8-wo *Fbp1*$^{F/F}$ and *Fbp1*$^{\Delta Hep}$ mice stained with the indicated antibody combinations.

(O-T) Quantification of representative PLA images of AKT-FBP1 (O), ALDOB-FBP1 (P), PP2A-C-FBP1 (Q), AKT-PP2A-C (R), AKT-ALDOB (S), and ALDOB-PP2A-C (T) interactions detected by PLA of liver sections from fasted 8-wo WT mice treated -/+ insulin (0.5U/kg) stained with the indicated antibody combinations.

(U) HK-2 and Caco-2 cells stably transfected with shCtrl or shFBP1 were treated -/+ insulin (100 nM) and IB'ed with indicated antibodies.

(V) In vitro dephosphorylation of HA-AKT1 isolated from insulin stimulated Huh7 cells and incubated with active-PP2A-C in the presence or absence of ALDOB. The reactions were IB analyzed with the indicated antibodies (left). Relative P-AKT (S473) and P-AKT (T308) intensity was determined by densitometry (right).

(W) HA-c-Myc was isolated from EGF (100ng/ml) stimulated stably expressing Huh7 cells incubated with active PP2A-C in the presence or absence of recombinant FBP1 and ALDOB. The reactions were IB analyzed with the indicated antibodies (left). Relative c-Myc (p-S62) intensity was determined by densitometry (right).

Data are presented as mean ± SEM. *P < 0.05, **P < 0.01, ***P < 0.001, ****p < 0.0001 (Unpaired two-tailed t test).

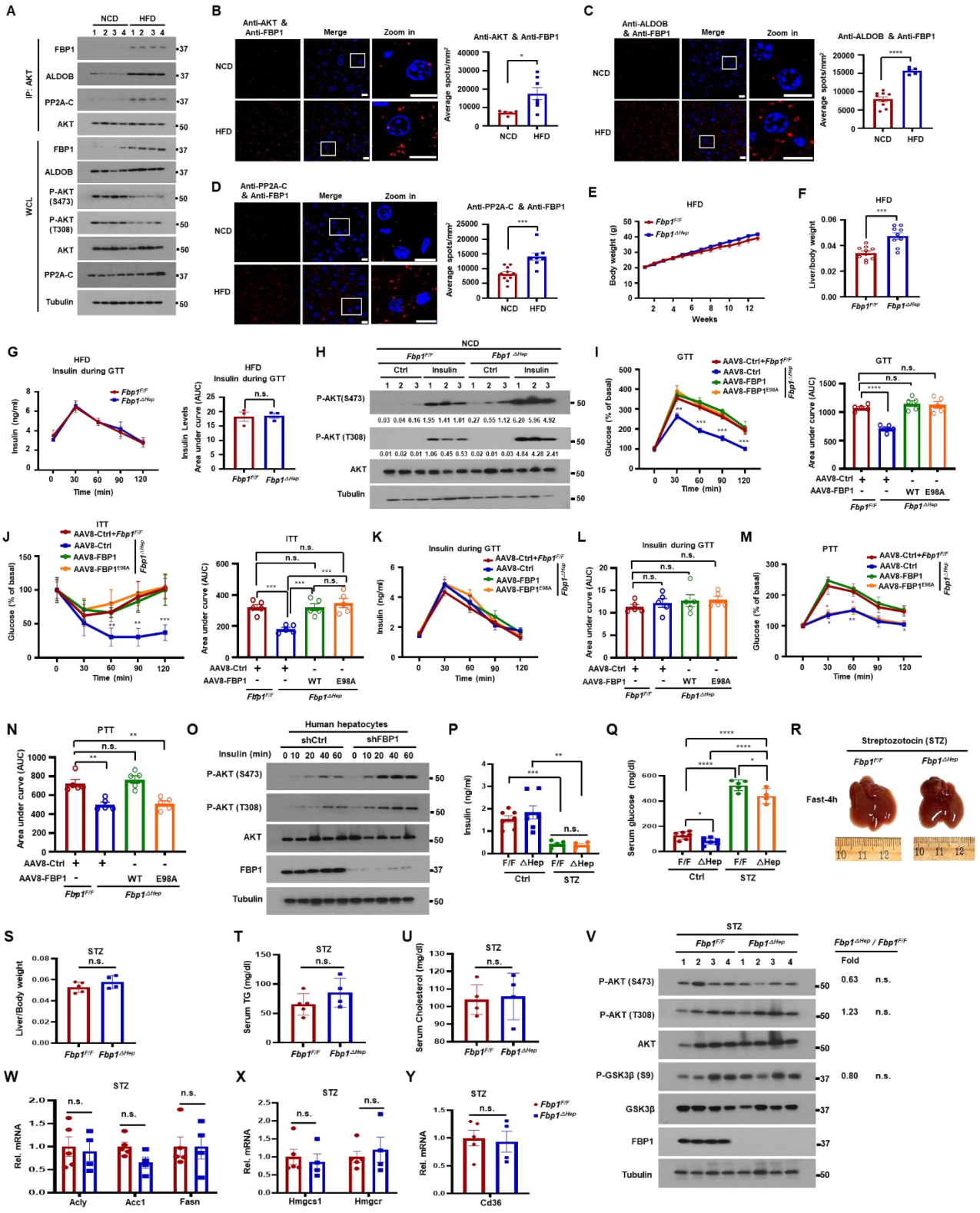

Figure S7. *Fbp1*$^{\Delta Hep}$ mice are insulin hyperresponsive, Related to Figure 6.

(A) IP analysis of liver lysates from 18-wo NCD and HFD fed WT mice. The gel separated IPs

were IB'ed with the indicated antibodies.

(B-D) Representative images of AKT-FBP1 (B, left), ALDOB-FBP1 (C, left) and PP2A-C-FBP1 (D, left) interactions detected by PLA of liver sections of NCD or HFD fed WT mice stained with the indicated antibody combinations. Scale bars, 10 µm. Quantification of the PLA signals is shown on the right.

(E) Body weight gain by HFD-fed *Fbp1*$^{F/F}$ and *Fbp1*$^{\Delta Hep}$ mice (n=9-10).

(F) Liver/body weight ratio in indicated HFD-fed mice (n=9-10).

(G) Insulin levels during the GTT shown Figure 6H (n=3) (left) and AUC quantification (right).

(H) IB analysis of NCD-fed 8-wo *Fbp1*$^{F/F}$ and *Fbp1*$^{\Delta Hep}$ liver lysates prepared 15 min after control or insulin injections. Relative normalized protein amounts are shown below the P-AKT strips.

(I and J) GTT (I, left) and ITT (J, left) performed on fasted *Fbp1*$^{F/F}$ and *Fbp1*$^{\Delta Hep}$ mice transduced with AAV8-Ctrl, AAV8-FBP1 or AAV8-FBP1^{E98A} (n=4-5). AUC quantification of glucose amounts (I and J, right).

(K and L) Insulin concentrations during GTT of the indicated mice (K) (n=4-5) and AUC quantification (L).

(M and N) Pyruvate tolerance test (PTT) performed on fasted *Fbp1*$^{F/F}$ and *Fbp1*$^{\Delta Hep}$ mice transduced with AAV8-Ctrl, AAV8-FBP1 or AAV8-FBP1^{E98A} (n=4-5) (M). AUC quantification of glucose amounts (N).

(O) Human hepatocytes stably transfected with shCtrl or shFBP1 were stimulated with insulin (100 nM) for the indicated times after 6 h serum starvation. The cells were lysed and IB analyzed with the indicated antibodies.

(P and Q) Serum insulin (P) and glucose (Q) of -/+ STZ treated *Fbp1*$^{F/F}$ and *Fbp1*$^{\Delta Hep}$ mice (n=4-7).

(R) Gross liver morphology of 4 h fasted STZ treated 8-wo *Fbp1*$^{F/F}$ and *Fbp1*$^{\Delta Hep}$ mice (n=4-6).

(S-U) Liver/body weight ratio (S), serum TG (T) and cholesterol (U) of STZ treated *Fbp1*$^{F/F}$ and *Fbp1*$^{\Delta Hep}$ mice from S7R (n=4-6).

(V) IB analysis of liver lysates of STZ treated and fasted *Fbp1*$^{F/F}$ and *Fbp1*$^{\Delta Hep}$ mice. Relative normalized protein ratios (*Fbp1*$^{\Delta Hep}$/*Fbp1*$^{F/F}$) and P values are shown on the right.

(W-Y) qRT-PCR of *Acly*, *Acc1, Fasn* (W), *Hmgcs1, Hmgcr* (X) and *Cd36* (Y) mRNAs in livers of STZ treated and fasted *Fbp1*$^{F/F}$ and *Fbp1*$^{\Delta Hep}$ mice (n=4-6).

Data are presented as mean ± SEM. *P < 0.05, **P < 0.01, ***P < 0.001, ****p < 0.0001, n.s., not significant (Unpaired two-tailed t test).

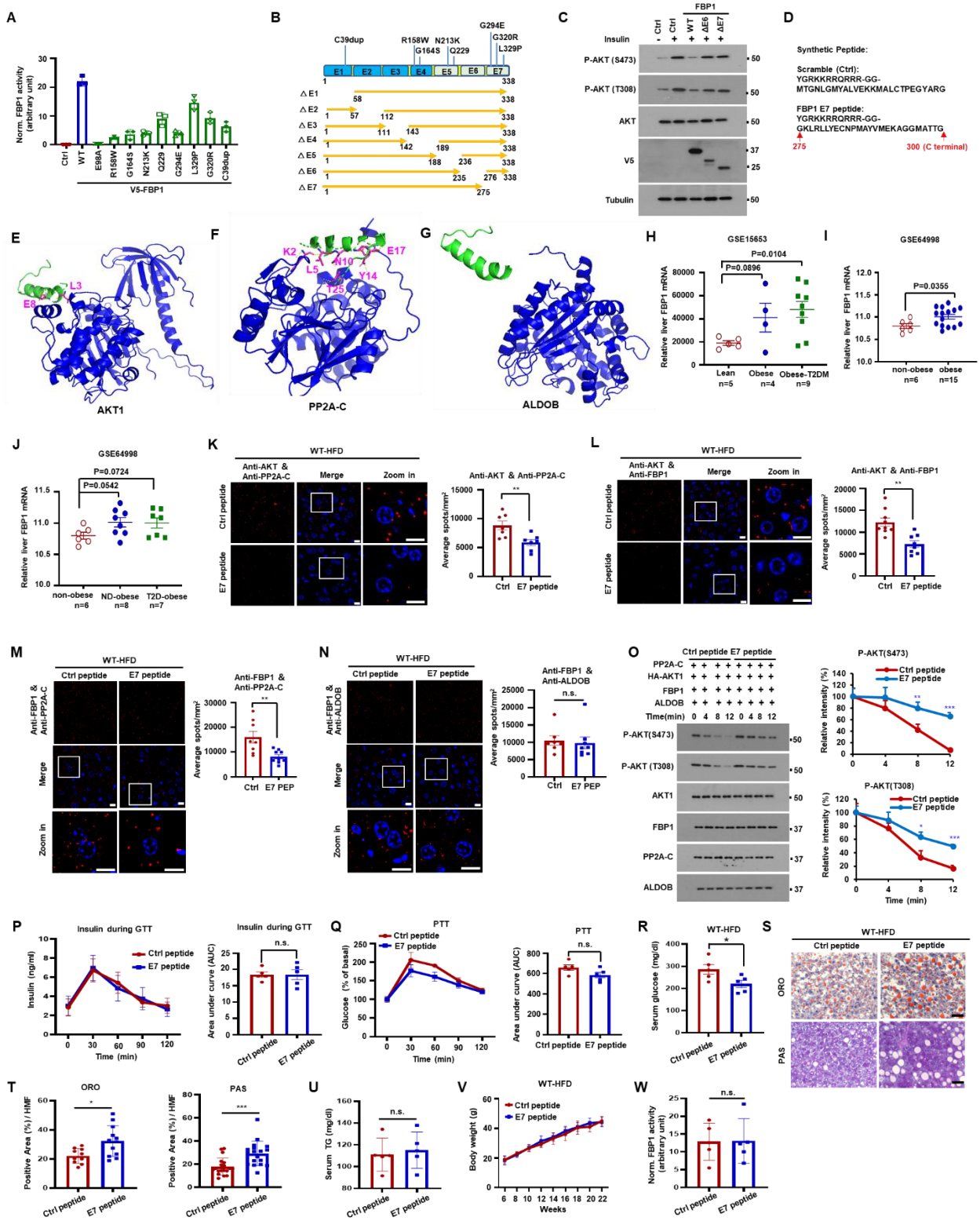

Figure S8. An FBP1 C-terminal peptide that disrupts FBP1:AKT:PP2A-C interactions activates AKT and ameliorates insulin resistance, Related to Figure 7.

(A) Normalized FBP1 enzyme activities of WT and missense human FBP1 mutants expressed in Huh7 cells.

(B) Schematic of FBP1 exon deletion mutants.

(C) Huh7 cells stably expressing the indicated proteins were treated with -/+ insulin (100 nM) and IB'ed with the indicated antibodies.

(D) The sequence of the cell permeable E7 peptide (preceded by the TAT peptide) corresponding to FBP1 AA 275-300. The scrambled peptide was used as a control.

(E-G) AlphaFold predictions of E7 peptide docking onto AKT1 (E), PP2A-C (F) and ALDOB (G).

(H-J) Relative *FBP1* mRNA levels according to GEO databases GSE15653 of livers from lean, obese and obese T2DM (H), GSE64998 of livers from non-obese and obese individuals (I), GSE64998 of livers from non-obese, ND-obese and T2D-obese individuals (J). T2DM, Type 2 diabetes. ND-obese, non-diabetic obese.

(K-N) Representative images of AKT-PP2A-C (K, left), AKT-FBP1 (L, left), FBP1-PP2A-C (M, left) and FBP1-ALDOB (N, left) interactions detected by PLA of liver sections of HFD-fed WT mice treated with Ctrl or FBP1 E7 peptides and stained with the indicated antibody combinations. Scale bars, 10μm. Quantification of representative PLA images is shown on the right.

(O) In vitro dephosphorylation of HA-AKT1 isolated from insulin stimulated Huh7 cells and incubated with active-PP2A-C in the presence or absence the E7 peptide. The reactions were IB analyzed with the indicated antibodies (left). Relative intensity of P-AKT (S473) and P-AKT (T308) was determined by densitometry (right).

(P) Insulin levels during the GTT from Figure 7H (left) and AUC quantification of the insulin levels (right) (n=5).

(Q) PTT performed on the HFD-fed mice from Figure 7D fasted for 12-14h (left) and AUC quantification (right).

(R) Serum glucose in mice from Figure 7D (n=5).

(S and T) ORO and PAS staining of liver sections from Figure 7D (S). Scale bars, 20 μm. ORO and PAS staining positive areas per HMF (T).

(U) Serum TG in mice from Figure 7D (n=5).

(V) Body weight gain of HFD fed mice treated with Ctrl and FBP1 E7 peptide (n=5).

(W) Normalized FBP1 activity in HFD fed mice from Figure 7D (n=5).

Data are presented as mean ± SEM. *P < 0.05, **P < 0.01, ***P < 0.001, n.s., not significant (Unpaired two-tailed t test).

Table S1. Primers for constructs used in this study, Related to STAR Methods.

Insert	Forward Primer (5'-3')	Reverse Primer (5'-3')
FBP1-R158W	GCAACCAGGCTGGAACCTGGT	AGAGCATCCTTCTCAGAAGGC
FBP1-G164S	GGTGGCAGCCAGCTACGCACT	AGGTTCCGGCCTGGTTGC
FBP1-N213K	ACAGCCTTAAGGAGGGCTACG	AGATTTTACCTTTCTTTTTTATCTTC ACATC
FBP1-Q229	TGAGTACATCTAGAGGAAGAAGT TC	GTGACGGCAGGGTCAAAG
FBP1-G294E	AAGGCTGGGGAAATGGCCACC	CTCCATGACGTAGGCCATG
FBP1-G320R	GGTGATCTTGAGATCCCCCGAC	GGCGCCCTCTGGTGAATG
FBP1-L329P	CTCGAGTTCCCGAAGGTGTATG AGAAGC	CACGTCGTCGGGGGATCC
FBP1-C39dup	CACTGCACAGCAGTCAAAGCC	CAGGAGCGAGTTGAGCAGCTGG

Table S2. shRNA and sgRNA sequences used in this study, Related to STAR Methods.

shRNA and sgRNA	Target Sequences（5'-3'）
sgALDOB#1	CACCGGATCACACCCCCGATGCTC
sgALDOB#2	CACCGGATTTCTCGGAACTGCCGG
shPP2A-C#1	TGGAACTTGACGATACTCTAA
shPP2A-C#2	CCCATGTTGTTCTTTGTTATT
shFBP1#1	CGACCTGGTTATGAACATGTT
shFBP1#2	CAGCAGTCAAAGCCATCTCTT

Table S3. Quantitative PCR primers used in this study, Related to STAR Methods.

Gene	Forward Primer (5’-3’)	Reverse Primer (5’-3’)
Acly	GCCAGCGGGAGCACATC	CTTTGCAGGTGCCACTTCATC
Acaca	TGACAGACTGATCGCAGAGAAAG	TGGAGAGCCCCACACACA
Fasn	GCTGCGGAAACTTCAGGAAAT	AGAGACGTGTCACTCCTGGACTT
Hmgcs1	GCCGTGAACTGGGTCGAA	GCATATATAGCAATGTCTCCTGCAA
Hmgcr	CTTGTGGAATGCCTTGTGATTG	AGCCGAAGCAGCACATGAT
Tkt	CGAAACCCTCACAATGATCG	TTCCTCAGGTTCAGCAGCTC
Pgd	ATGCCAGGAGGGAACAAAG	GTTCTCCGGTTCCCACTTTT
Glut2	TGCTGGCCTCAGCTTTATTC	TTTCTTTGCCCTGACTTCCTC
Pkm2	GCTA TTCGAGGAACTCCGCC	AAGGTACAGGCACTACACGC
Me1	GATGATAAGGTCTTCCTCACC	TTACTGGTTGACTTTGGTCTGT
Mthfd2	ACAGATGGAGCTCACGAACG	TGCCAGCGGCAGATATTACA
Ppat	AATAGCTGTGGCCCATAACG	ACGTGGAAAGCCCAATACC
Gbe1	GCGATCATGGAACATGCTTACTAT	CCATAACGACTTGAAGCTGCAA
Cpt1α	TGTCCAAGTATCTGGCAGTCG	CATAGCCGTCATCAGCAACC
Cpt2	ATCGTACCCACCATGCACTAC	CTGTCATTCAAGAGAGGCTTCTG
Srebp1c	GGAGCCATGGATTGCACATT	GGCCCGGGAAGTCACTGT
Cd36	TCCTCTGACATTTGCAGGTCTATC	AAAGGCATTGGCTGGAAGAA